

Intraseasonal variability of equatorial Indian Ocean zonal currents

Debasis Sengupta¹, Retish Senan² and B. N. Goswami

Centre for Atmospheric and Oceanic Sciences

Indian Institute of Science, Bangalore, India

Jérôme Vialard

Institut de Recherche pour le Développement

Laboratoire d'Océanographie et de Climat par Expérimentation et Approche Numérique

Université Pierre et Marie Curie, Paris, France

To appear in J. of Climate

Submitted 15 March 2005

Revised 10 November 2005

Accepted 30 November 2005

¹*Corresponding author address:* Debasis Sengupta, Centre for Atmospheric and Oceanic Sciences, Indian Institute of Science, Bangalore 560012, India. E-mail: dsen@caos.iisc.ernet.in

²*Presently at* Laboratoire d'Océanographie et de Climat par Expérimentation et Approche Numérique, Université Pierre et Marie Curie, Paris, France

Abstract

New satellite and *in situ* observations show large intraseasonal (10-60 day) variability of surface wind and upper ocean current in the equatorial Indian Ocean, particularly in the east. We use an ocean model forced by QuikSCAT scatterometer wind stress to study the dynamics of intraseasonal zonal current. The model has realistic upper ocean current and thermocline depth variability on intraseasonal to interannual scale. The quality of the simulation is directly attributed to the accuracy of the wind forcing. At the equator, moderate westerly winds are punctuated by strong 10-40 day westerly wind bursts. The wind bursts force swift, intraseasonal (20-50 day) eastward equatorial jets in spring, summer and fall. Zonal momentum balance is between local acceleration, stress and pressure; nonlinearity deepens and strengthens eastward current. Westward pressure force associated with thermocline deepening toward the east rapidly arrests eastward jets, and subsequently generates (weak) westward flow. Thus, in accord with direct observations in the east (Masumoto et al. 2005), the spring jet is a single intraseasonal event, there are intraseasonal jets in summer, whereas the fall jet is long lived but strongly modulated on intraseasonal scale. Zonal pressure force is almost always westward in the upper 120 m, and changes sign twice a year in the 120-200 m layer. Transient eastward equatorial undercurrents in early spring and late summer are associated with semiannual Rossby waves generated at the eastern boundary following thermocline deepening by the spring and fall jets. Easterly wind stress is not necessary to generate the undercurrents. Experiments with a single westerly wind burst forcing show that apart from the intraseasonal response, zonal pressure force and current in the east have an intrinsic 90-day time scale that arises purely from equatorial adjustment.

1. Introduction

The availability of new high frequency satellite winds and *in situ* observations is an important development in the study of the equatorial Indian Ocean (EqIO) because they resolve subseasonal variability (Sengupta et al. 2004; Masumoto et al. 2005). Accurate estimates of surface wind with high time and space resolution from the scatterometer on QuikSCAT are available since July 1999 (Liu 2002; Chelton et al. 2001). The first direct observations of surface wind, upper ocean current and temperature in the eastern EqIO began soon after. The National Institute of Oceanography (NIO), Goa, has deployed a series of moored subsurface current meters beginning February 2000 at $0^\circ, 93^\circ\text{E}$, $0^\circ, 83^\circ\text{E}$ and $0^\circ, 77^\circ\text{E}$ (Murty et al. 2002). The Japan Marine Science and Technology Center, JAMSTEC, deployed a moored Acoustic Doppler Current Profiler (ADCP) in November 2000 at 400 m depth, $0^\circ, 90^\circ\text{E}$ (Masumoto et al. 2005), and a TRITON (TRIangle Trans-Ocean buoy Network) buoy in October 2001 at $1.6^\circ\text{S}, 90^\circ\text{E}$ (Kuroda 2002). Ongoing observations from these instruments already cover a longer period than earlier *in situ* time series measurements in the EqIO, including those from Gan (Knox 1976; McPhaden 1982), the western EqIO (Luyten and Roemmich 1982) and south of Sri Lanka (Schott et al. 1994; Reppin et al. 1999).

Here we use an ocean general circulation model forced by 1999-2003 three-day QuikSCAT winds, validated against available data, to study the basic dynamics of intraseasonal zonal current in the upper 200 m of the EqIO. Although the emphasis is on intraseasonal variability, we revisit some questions related to dynamics of the seasonal cycle.

a. Seasonal Jets and Undercurrents

The Gan data showed that eastward equatorial jets (Wyrтки 1973; Shenoi et al. 1999) accelerate to about 1 m s^{-1} when westerly wind stress abruptly increases in spring and fall, but decelerate while the wind stress continues to be westerly; each jet is followed by westward flow in the upper ocean lasting a month or longer. From the observed winds and currents at Gan, Knox (1976) deduced that the jets are accelerated by zonal wind stress, but decelerated by time varying zonal pressure gradient (ZPG). He suggested that the westward pressure force required for momentum balance arises because westerly wind stress temporarily raises sea level in the east relative to the west. Knox's estimate of the ZPG is broadly consistent with the difference of sea level between the eastern and western equatorial Indian Ocean. Historical sea level data show that this difference reaches its largest value (about 0.2 m) in June and December, following the eastward equatorial jets (Wyrтки 1973).

A climatology of basin-scale ZPG in the upper 200 m of the EqIO has been constructed by Bubnov (1994), based on hydrographic data from 1962-1988 along 51 equatorial sections between 55°E and 90°E . Estimates based on dynamic topography show that ZPG in the upper 100 m is eastward (i.e. the pressure force is westward) throughout the year except in February and March. The seasonal cycle of ZPG in the upper 100 m has practically the same phase as the equatorial zonal wind stress, with a dominant semiannual period. The ZPG in June and December (about $5 \times 10^{-7} \text{ N kg}^{-1}$, or m s^{-2}) corresponds to an east-west sea level difference of about 0.2 m. In February and March the pressure force in the upper 200 m is eastward, with a maximum at 100 m depth of about $-2.0 \times 10^{-7} \text{ N kg}^{-1}$, comparable to that in the equatorial Atlantic or Pacific.

ZPG associated with equatorial Kelvin and Rossby waves generated/reflected at lateral boundaries determine ocean adjustment to uniform westerly wind stress. Since eastward jets are surface intensified, it has been argued that these waves must have vertical structure resembling the second baroclinic mode (Philander and Pacanowski 1980). Semiannual subsurface zonal current (u) in the Gan and Sri Lanka data has upward phase propagation, evidence of free waves carrying energy to deeper levels (McPhaden 1982; Reppin et al. 1999). A strong semiannual signal in the subsurface u record from the western EqIO has been interpreted as vertically propagating first meridional mode Rossby waves, with zonal wavelength of several thousand kilometers and westward propagation speed of about 0.5 m s^{-1} (Luyten and Roemmich 1982). Many features of the western EqIO semiannual u signal can be understood in terms of equatorial waves forced by semiannual zonal wind stress in the presence of lateral boundaries; although the second baroclinic mode is important, several vertically standing modes are required to account for the observed vertical phase propagation (Gent et al. 1983). Le Blanc and Boulanger (2001) suggest that much of the seasonal to interannual variability of TOPEX/POSEIDON sea surface height in the EqIO can be interpreted in terms of wind forced Kelvin waves and first meridional mode Rossby waves, and their reflection at lateral boundaries. The speed of the Kelvin wave in the sea level data is 2 m s^{-1} to the east, while the long Rossby wave moves west at 0.7 m s^{-1} . Note that the meridional structure of sea level associated with an eastward equatorial jet projects strongly onto that of a downwelling Kelvin wave. Secondly, since sea level changes project preferentially into first baroclinic ($n=1$) equatorial waves, analysis based on sea level alone is likely to underestimate the importance of the second ($n=2$) and higher modes.

Eastward equatorial undercurrents (EUC, defined as eastward current in the thermocline be-

neath upper ocean westward flow) in the Indian Ocean are transient features related to wave dynamics (Schott and McCreary 2001, hereafter SM). Several observations in the central and western EqIO show eastward EUC's in February-May, but they have been reported also during June-August (Bubnov 1994). Apart from the eastward EUC in March-May 1994 in the Sri Lanka data, there is eastward flow at 50-150 m depth in August-September 1994, but not in 1993 (Reppin et al. 1999). The ADCP zonal current in the eastern EqIO consistently shows eastward EUC's in both seasons - between December-April and June-September (Masumoto et al. 2005). Subsurface u alternates between eastward and westward flow with broadly semiannual period and upward phase propagation. Each distinct eastward EUC is preceded by upward phase propagation of semiannual eastward u .

Most previous studies of equatorial Indian Ocean circulation address the climatological seasonal cycle (e.g. Gent et al. 1983; McCreary et al. 1993; Anderson and Carrington 1993) or interannual variability (e.g., Reverdin et al. 1986; Saji et al. 1999; Murtugudde et al. 1999; Schiller et al. 2000). The seasonal cycle of surface zonal current, in particular the dominant semiannual period, is determined by the phase relation between directly wind-driven flow and flow associated with waves (Han et al. 1999). In other words, the seasonal cycle of u depends on the phase relation between time varying zonal wind stress and time varying zonal pressure force. The strength of the eastward jets in models is sensitive to the choice of wind stress climatology (Anderson and Carrington 1993) and the depth of the mixed layer (Han et al. 1999; Masson et al. 2004). Models forced by climatological winds consistently generate a transient eastward EUC in spring. For example, the McCreary et al. (1993) solution has an eastward EUC with a core at thermocline depth in January-March. Some models (e.g. Anderson and Carrington 1993) also have an east-

ward EUC in August-September. Although EUC's arise from dynamical adjustment to westerly winds, several observational and modelling studies note that the spring EUC follows a spell of easterly winds in the EqIO (SM; Godfrey et al. 2001). It is not clear from the published literature if easterly winds are essential to generate the semiannual EUC in the Indian Ocean. Sustained easterly winds during late 1997 forced westward surface currents at the equator, equatorial upwelling and a swift eastward EUC (Murtugudde et al. 2000). Basin wide sea level anomalies in the tropical Indian Ocean, associated with propagating waves, persist for two seasons or more during dipole events (Webster et al. 1999). The large scale sea level anomalies in 1993/1994 or 1997/1998 (Le Blanc and Boulanger 2001) imply anomalous zonal pressure gradients in the equatorial ocean (Grotsky et al. 2001). Upper ocean pressure is essentially in phase with wind stress on interannual as well as semiannual time scales.

b. *Intraseasonal Variability of Zonal Current*

It has been known for some time that upper ocean currents in the EqIO have substantial intraseasonal variability. For example, the weekly current data at Gan has u variability at 30-60 day period, and some evidence of sub-monthly variability. McPhaden (1982) suggests that the 30-60 day variability is wind forced, because it is coherent with variability of zonal wind stress. The 1993 fall jet in the Sri Lanka data is deep, swift, long-lived and modulated on intraseasonal time scale (Reppin et al. 1999). Equatorial u south of Sri Lanka has spectral peaks at 30-50 day, 22 day and 15 day period, whereas equatorial v and off-equator u have a peak at 15 days (SM). The new direct measurements suggest that intraseasonal variability dominates upper ocean currents

in the eastern EqIO. In the JAMSTEC ADCP data, for example, the amplitude of 30-50 day u variability at 40m depth is 0.5 m s^{-1} , compared to a 0.1 m s^{-1} semiannual signal; the dominant variability of v has 10-20 day period (Masumoto et al. 2005). The NIO subsurface current data (shallowest instrument at 100 m) also shows dominant 30-60 day u variability, and a distinct 10-20 day oscillation of v at all depths (Murty et al. 2002; Sengupta et al. 2004).

There are relatively few model studies of the dynamics of intraseasonal variability of Indian Ocean circulation. Moore and McCreary (1990) showed that 40-50 day variability in the western EqIO can be wind forced, whereas other studies attribute intraseasonal variability in this region to dynamic instability of western boundary currents (SM). The work of Sengupta et al. (2001) focuses mainly on intraseasonal variability of off-equatorial zonal currents in the region south and east of Sri Lanka, not on equatorial currents. (Han et al. 2001; Han 2005) show that the 30-60 day variability of zonal current is directly wind forced, and report a dominant 90 day peak in observed sea level in the eastern EqIO, as well as model upper ocean current. The 90 day variability is attributed to selective response (“resonance”) of the ocean to weak 90-day wind variations. We have previously demonstrated the important role of ZPG in the existence of intraseasonal jets in the EqIO - westerly wind bursts generate intraseasonal jets in summer, but not in winter because the stress is overcome by westward pressure force (Senan et al. 2003). The findings of these studies are discussed later in the context of our results.

Recent work suggests that intraseasonal variability of upper ocean currents is relevant to regional climate. For example, Loschnigg and Webster (2000) and Waliser et al. (2004) suggest that wind forced intraseasonal currents make a significant contribution to ocean heat transport and upper ocean heat balance. Other studies propose that intraseasonal variability influences In-

dian Ocean temperature distribution on longer time scales (Schiller and Godfrey 2001; Waliser et al. 2004; Sengupta et al. 2004; Han 2005). On the other hand, intraseasonal variability of zonal winds and currents is influenced by large scale seasonal variations of the tropical atmosphere and ocean (Chatterji and Goswami 2004; Senan et al. 2003). Observations and models suggest that the 10-60 day variability of wind, currents and SST in the Indian ocean (Sengupta et al. 2001; Vecchi and Harrison 2002; Saji et al. 2005) involves air-sea interaction (e.g., Zheng et al. 2004; Fu et al. 2003b). The role of air sea interaction in intraseasonal variability of Indian Ocean climate is an active area of research (see the reviews of Webster et al. 1998; Goswami 2005; Waliser 2005).

This paper is organised as follows. Results from the QuikSCAT simulation are compared with available observations, and with a simulation forced by daily NCEP reanalysis winds. We find that high quality wind forcing leads to realistic simulation of large-scale zonal currents in the EqIO. Experiments with idealised wind forcing aid dynamical interpretation of the intraseasonal variability of u . The model setup and the main experiments are described in the next section. In section 3 we demonstrate the ability of the model to simulate the major observed features of equatorial circulation, and discuss the large scale variability of winds and currents. The dominant balance of forces that determines the evolution of equatorial zonal flow is examined in section 4. This explicit calculation demonstrates the central importance of rapidly varying zonal pressure force. The relevance of the experiments with idealized winds is also discussed in this section. Section 5 summarises the main conclusions.

2. The Model

We use the Modular Ocean Model 2.2 (Pacanowski 1996) with Indian Ocean domain (30°S-30°N and 30°E-110°E), having a sponge layer at 30°S and a wall at 110°E. Horizontal resolution is approximately $1/3^\circ$ by $1/3^\circ$ north of 5° S. There are 19 levels in the vertical, six of which are in the top 100 metres. Horizontal eddy diffusivity and viscosity are $2000 \text{ m}^2 \text{ s}^{-1}$. Vertical mixing is based on the scheme of Pacanowski and Philander (1981). Topography is based on the $1/12^\circ$ data from the U.S. National Geophysical Data Center. No explicit surface fluxes of heat or freshwater are used to force the model. Surface temperature and salinity fields are relaxed to the observed annual cycle from the climatological data of Levitus (1982), with an e-folding timescale of 10 days.

Several model runs or experiments were performed; a list is given in Table 1. In the *control* run, or the QuikSCAT simulation, the model is forced by July 1999-December 2003 three-day wind stress obtained from $0.25^\circ \times 0.25^\circ$ QuikSCAT vector winds using a constant drag coefficient C_d of 1.2×10^{-3} . This wind stress field has almost no gaps due to limited satellite swath (about 1,500 km) or rain. A test run with an objectively interpolated daily gridded ($1^\circ \times 1^\circ$) wind stress field created from QuikSCAT winds (Pegion et al. 2000) gives almost identical results. The initial conditions for the *control* run, on 20 July 1999, came from a 15 year simulation of the model (“NCEP” run) with daily surface wind stress derived from the NCEP/NCAR reanalysis (Kalnay et al. 1996) surface winds using the same C_d . The model has been forced with a low pass version wind stress, obtained from the daily 1999-2002 QuikSCAT wind stress by removing all variability with periods less than 90 days. We call this the *seasonal* run. In addition to the

control and *seasonal* runs, we use results from several sensitivity experiments with the model ocean forced by idealized wind stress fields (Table 1) - these are further described in section 4.

3. Variability of Equatorial Zonal Currents

a. Comparison with Observations

Daily data from the TRITON mooring (<http://www.jamstec.go.jp/jamstec/TRITON/>) shows that relative to the amplitude of the seasonal cycle, intraseasonal variability of wind and current is stronger in the eastern EqIO than at Gan (Knox 1976). The root mean square (rms) difference between weekly equivalent-neutral QuikSCAT windspeed and *in situ* TRITON windspeed is about 1 m s^{-1} . The QuikSCAT zonal wind stress is accurate, but slightly overestimates maximum stress (Figure 1a). The phase of intraseasonal variability of 10 m zonal current from the QuikSCAT simulation compares reasonably well with 10 m u from TRITON data (Figure 1b), although peak speeds can be higher in the model. The depth of the 20° isotherm ($d20$) from the model and TRITON observations are close, but occasionally model $d20$ can be 10-15m too shallow for upto a month (Figure 1c).

The variability of zonal pressure gradient at the equator computed from model surface dynamic height is reasonably close to that estimated from TOPEX/Poseidon (Fu et al. 1994) and Jason-1 (Fu et al. 2003a) sea surface height (Figure 2). The rms difference of 10-day model ZPG and satellite ZPG is $0.9 \times 10^{-7} \text{ m s}^{-2}$, compared to the standard deviation of daily model ZPG of $2.2 \times 10^{-7} \text{ m s}^{-2}$. The time average of September 1999-December 2003 model surface ZPG, equal to $4.26 \times 10^{-7} \text{ m s}^{-2}$, has been removed from the time series in Figure 2. If

the slope were uniform, this would correspond to a sea level difference of about 0.2 m between 95°E and 60°E. For comparison, Bubnov's estimate of annual mean surface ZPG is $3.8 \times 10^{-7} \text{ m s}^{-2}$. The anomalous dipole related ZPG of October 1997-March 1998 represents negative surface slope (east lower than west). Although the satellite sea levels are ten day datasets, they do show intraseasonal variability of zonal slope.

The depth-time evolution of zonal flow at 0°, 90°E in the model and JAMSTEC ADCP observations (Masumoto et al. 2005) agree in all major respects (Figure 3):

1. Eastward equatorial jets extend to a depth of about 120 m in both observations and model.
2. The spring jet is a single event with a lifetime of 30-50 days at this longitude; the fall jet is longer lived than the spring jet, and is modulated on intraseasonal time scales;
3. There are one or two intraseasonal eastward equatorial jets every summer . These “monsoon jets” (Senan et al. 2003) have a lifetime of about a month.
4. Subsurface zonal flow between 120 m and 200 m is generally eastward from January-April and July-September.
5. Westward subsurface flow in October-December and May-June, and eastward subsurface flow in January-February, appear first at deeper levels in the east.

The full ADCP record, November 2000-July 2003, is shown in Y. Masumoto (Observational activities for Studies on the Indian Ocean Climate System; http://www.jamstec.go.jp/frcgc/jp/sympo/2004/seika040428/ppt/10_CVORP_IO.pdf). In accord with the observations, the swiftest

eastward jets in the model are in spring 2002 and 2003. The fall 2002 jet consists of three nearly distinct intraseasonal events.

The model has certain systematic shortcomings. The model fall jets are somewhat stronger, and more persistent than observed. It is likely that westerly wind stress is overestimated because stress is not calculated from wind relative to ocean surface current (M. J. Harrison 2004, personal communication). Model subsurface currents are somewhat weaker than observed; in particular, the model eastward undercurrent at 75-150 m depth are weaker than observed in April 2002 and March-April 2003. Comparison with temperature from the NIO mooring at 0° , 93°E suggests (Sengupta et al. 2004) that the model vertical gradient of thermocline temperature is realistic. However, away from the equator at the location of the TRITON mooring (Figure 1c), the model does not reproduce the nearly 100 m deep isothermal layer in some seasons. Occasionally, model 100 m temperature is too cool by $2\text{-}3^\circ\text{C}$, and the thermocline more diffuse than observed (not shown). These limitations might be due to the relatively coarse model vertical resolution (about 25 m) below 100 m depth, as well as deficiencies in mixing parameterisation.

The equatorial Indian Ocean circulation is rather sensitive to the choice of wind product used to force the model, consistent with the findings of Anderson and Carrington (1993). Westerly winds in the EqIO are weak in the NCEP reanalysis product compared to QuikSCAT throughout the year, particularly in the east (Figure 4a). Seasonal mean windspeed as well as intraseasonal variability of zonal wind is underestimated in the reanalysis product. Goswami and Sengupta (2003) suggest that this is related to inaccurate representation of atmospheric convective heating over the eastern tropical Indian Ocean in the NCEP model. As a consequence, the fall jet and the intraseasonal jets in the NCEP run are weak in the eastern EqIO (Figure 4b). The correla-

tion coefficient between TRITON and model 10m u is 0.73 for the QuikSCAT run and 0.60 for the NCEP run. The NCEP run 100 m temperature is systematically too cool compared to the QuikSCAT simulation (Figure 4c); NCEP $d20$ is 20 m too shallow relative to QuikSCAT $d20$ at the equator, or to TRITON $d20$ away from the equator throughout the year, except in spring (not shown). The TRITON-model $d20$ correlation coefficient is 0.94 for QuikSCAT and 0.80 for NCEP. Note that surface heat and freshwater fluxes are not externally prescribed, but come purely from relaxation to climatology. We conclude that the model can simulate equatorial Indian Ocean circulation with reasonable fidelity provided the surface wind forcing is accurate. This is a major result of the present study.

b. Variability of Wind, Current and Pressure Gradient

Before taking up the dynamics of zonal current in Section 4, we briefly describe variability of the wind stress and zonal current fields in the north Indian Ocean, as well as the variability of zonal pressure gradient in the equatorial region. The seasonal cycle of QuikSCAT zonal and meridional wind stress has largest amplitude off the African coast and in the Arabian Sea, exceeding 0.08 N m^{-2} . The seasonal cycle of model upper ocean zonal current is largest in the western boundary regions off Africa and the east coast of India. In the equatorial waveguide, the amplitude of the seasonal cycle is $0.2\text{-}0.4 \text{ m s}^{-1}$ (not shown). Intraseasonal zonal wind stress (τ_x) variability is largest (daily standard deviation $> 0.03 \text{ N m}^{-2}$) in the central Arabian Sea and Bay of Bengal, south of Sri Lanka and east of 75°E in the EqIO (Figure 5a). Equatorial westerly wind bursts lasting 10 to 40 days occur throughout the year (Figure 1; Figure 5 of Knox (1976)), in response

to intraseasonal variations of organised atmospheric convection (Goswami and Sengupta 2003). Intraseasonal variability of upper ocean u is largest in the equatorial waveguide. Its amplitude exceeds the seasonal variability at 90°E , consistent with the finding of Masumoto et al. (2005) (Figure 5b). There is some intraseasonal variability of u in the *seasonal* run, with maximum amplitude of $0.04\text{--}0.08 \text{ m s}^{-1}$ in the EqIO and off Africa (not shown), which arises from dynamic instability of seasonal currents (Vinayachandran et al. 1996; Sengupta et al. 2001). The contribution of instability to intraseasonal variance of u in the EqIO is generally 10-20% in moderate horizontal resolution models, except west of 55°E where it can reach 30-40% (Han et al. 2004).

Figure 6 shows three day and seasonal QuikSCAT τ_x , and daily upper ocean (0-120 m) and subsurface (120-200 m) zonal current, averaged over $60^\circ\text{E}\text{--}95^\circ\text{E}$, from the *control* and *seasonal* runs. QuikSCAT zonal wind stress within a few degrees of the equator is almost always westerly. Episodes of westerly wind stress are generally, but not always, followed by upper ocean eastward flow. Similarly, there is no one-to-one relation between easterly wind stress and either upper ocean westward flow, or subsurface eastward flow. The subsurface zonal flow is generally eastward; westward flow persists upto three months in October-January and May-July, with substantial year-to-year differences. Equatorial “undercurrents”, with eastward flow lying underneath westward flow, occur twice every year.

The zonal extent of westerly wind bursts in the equatorial Indian Ocean is generally comparable to the basin size in spring and fall (Figure 7a). It is smaller in summer, with strong wind bursts mainly east of 75°E . Major westerly wind bursts ($\tau_x > 0.06 \text{ N m}^{-2}$) rarely last more than 40 days, and occasionally propagate eastward. Eastward equatorial jets in the upper ocean are longer lived in fall than in spring (Figure 7b), in agreement with the new time series observations

(Masumoto et al. 2005) and surface drifter climatology (Shenoi et al. 1999). Outside the fall season, strong eastward flow ($u > 0.8 \text{ m s}^{-1}$) has a lifetime of less than 40 days at any longitude. Subsurface (120-200 m) u is eastward much of the time (Figure 7c). Westward flow appears first at the eastern boundary at about the same time as strong eastward jets in the upper ocean. The envelope of westward u generally propagates west at $0.5\text{-}0.8 \text{ m s}^{-1}$. Many of these characteristics of the response of equatorial current to wind stress forcing are examined later in the paper.

Power spectra of July 1999-December 2003 zonal wind stress, zonal current and zonal pressure gradient from the *control* run show a dominant semiannual cycle and intraseasonal variability. We show variance preserving spectra (Chatfield 1975) in order to emphasise the intraseasonal scale relative to the semiannual. Most of the intraseasonal variance is at 30-60 day period (Figure 8). All quantities used in the spectrum calculations, including zonal pressure gradient, are from the model term balances, which represent daily time and volume averages of terms in the zonal momentum equation at each grid point and time step. Semiannual variance of τ_x is comparable in the east and west, whereas intraseasonal variance of τ_x is larger in the east (Figure 8a, 8b). The variability of zonal pressure gradient is much stronger in the east at all periods. Intraseasonal variability of u is also higher in the eastern EqIO (Figure 8c, 8d). Note that although there is a spectral valley between intraseasonal and semiannual τ_x , intraseasonal variability of upper ocean u or ZPG in the east is not clearly separated from variability with periods longer than 60 days. The spectral peaks of subsurface ZPG in the east lie at 40-60 day and 80-100 day periods (Figure 8f). We offer a dynamical explanation in the next section. Meridional currents are not discussed here. Information about the annual cycle of (τ_y) and v can be found in (Schott et al. 2002) and Godfrey et al. (2001), and about 10-20 day variability in (Sengupta et al. 2004).

4. Dynamics of Zonal Currents

a. Zonal Momentum Balance

We examine the zonal momentum balance in the QuikSCAT simulation in the equatorial strip 60°E-95°E, 1°S-1°N. The western edge is chosen at 60°E because the dynamics of the flow might be expected to be different in the western boundary region. For simplicity we denote the various terms in Cartesian coordinates. The model stress term is $\frac{\partial}{\partial z} \left(\kappa \frac{\partial u}{\partial z} \right)$, where z is depth and κ the coefficient of vertical momentum mixing; integration of the stress from a sufficiently deep level to the surface gives the model surface boundary condition

$$\kappa(z=0) \frac{\partial u}{\partial z} \Big|_{z=0} = \tau_x. \quad (1)$$

The stress is negligible below 120 m depth, except when there is a strong equatorial jet in the upper ocean (see below). The pressure acceleration, $\frac{-1}{\rho} \frac{\partial p}{\partial x}$, where ρ is density, p pressure and x eastward coordinate, is almost always westward in the upper 120 m. It is generally small or weakly eastward twice a year, and westward for three-four months following strong westerly winds in spring and fall (Figure 9a). Like wind stress or upper ocean current, zonal pressure force has a clear semiannual period, consistent with the climatology of (Bubnov 1994). The dominant zonal momentum balance is (Figure 9b)

$$\frac{\partial u}{\partial t} = -\frac{1}{\rho} \frac{\partial p}{\partial x} + \frac{\partial}{\partial z} \left(\kappa \frac{\partial u}{\partial z} \right). \quad (2)$$

Zonal acceleration is generally somewhat larger than the right hand side of equation (2). The vertical advection term $-w\frac{\partial u}{\partial z}$ is almost always positive, where w is vertical velocity (positive upwards), and exceeds the generally negative meridional advection $v\frac{\partial u}{\partial y}$ (Figure 9c). Our upper ocean box is relatively deep (120 m), but the net effect of nonlinearity is to strengthen and deepen eastward current, in agreement with past studies (Cane 1980). The zonal advection, horizontal mixing and Coriolis terms are generally smaller than vertical and meridional advection. Zonal advection is occasionally important - it is generally negative in the western and central EqIO but positive in the east, strengthening and prolonging eastward jets. Westerly wind bursts can lead to rapid change of zonal pressure force via equatorial waves. The lag correlation between 1999-2003 daily τ_x in the central EqIO (70°E-80°E) and 0-120m ZPG in the eastern EqIO (80°E-95°E) has a peak of 0.6 at 15 day lag. Therefore pressure has considerable intraseasonal variability (Figure 8). It can also change abruptly, as in late September 2001 and late April 2003, when it decreases by $4.0 \times 10^{-7} \text{ m s}^{-2}$ or more in a week. Examination of the spatial structure of the winds suggests that such large, rapid changes of ZPG are due to Kelvin waves generated in mid-basin by zonally nonuniform wind bursts.

The nature of the upper ocean dynamical balance, and the intraseasonal variability of the terms, has important consequences. For example, the eastward jets of spring 2002 and 2003 are swift (Figure 3) partly because the pressure force prior to these events is close to zero (Figure 6), and does not oppose eastward acceleration. The role of pressure also helps to explain a peculiar feature in the NCEP simulation. Although the April-May westerly wind bursts are somewhat weaker in NCEP than in QuikSCAT, the speed of the spring jets are comparable in the NCEP and QuikSCAT *control* runs (Figure 4). The fall jets, and the subsequent westward pressure force,

are much weaker in the NCEP simulation, favouring stronger spring jets (not shown). Eastward equatorial jets are accelerated to high speed within days of onset of westerly winds (Knox 1976; Philander and Pacanowski 1980). Our results (Figures 7b, 9b) suggest that jets are decelerated by the pressure gradient force (Cane 1980) within days of the weakening of westerly wind bursts. This is the basic dynamical reason why the response of the equatorial Indian Ocean to a westerly wind burst is an intraseasonal eastward jet (Masumoto et al. 2005). However, every burst does not generate a jet. Westerly bursts in June and July generate intraseasonal eastward jets in the eastern EqIO, but westerly bursts later in summer, or in winter (albeit rare) do not, because the pressure driven current in these periods is generally westward (Senan et al. 2003).

In the subsurface layer (60°E-95°E, 1°S-1°N and 120-200 m), stress is generally quite small or zero, except when there is a swift equatorial jet in the upper ocean (Figure 9d). Subsurface pressure force changes sign on semiannual time scales. It is westward following the major spring and fall jets, and eastward at other times. Zonal acceleration is small (its magnitude is less than $2.0 \times 10^{-7} \text{ m s}^{-2}$) compared to the upper ocean. The dominant balance is generally $\frac{\partial u}{\partial t} = \frac{-1}{\rho} \frac{\partial p}{\partial x}$, although occasionally there is substantial contribution from stress. In the fall of 1999 and 2001, for instance, the vertical diffusion of eastward zonal momentum from the upper layer reaches $1.2 \times 10^{-7} \text{ m s}^{-2}$. The vertical advection term generally accelerates eastward flow in the subsurface layer as well, although it is countered by meridional advection (Figure 9d). The horizontal mixing and Coriolis terms are small (not shown). Based on the observed eastward time mean u at all depths upto 200m at Gan, McPhaden (1982) deduced that nonlinearity is important in EqIO dynamics at thermocline depths (Eriksen 1979; Philander and Pacanowski 1980; Cane 1980). The nonlinearity of the momentum balance makes it likely that intraseasonal current

variability rectifies onto longer time scales (Waliser et al. 2004; Han 2005). Note that our model has restoring conditions on sea surface temperature and salinity. Therefore it is not suitable to study rectification, which involves among other things the interaction of wind stress and mixed layer depth changes.

As most existing model studies of the Indian Ocean use monthly mean wind forcing, it is instructive to examine the dynamics of upper ocean zonal current in the *seasonal* experiment, where the wind stress has no subseasonal variability. The dominant zonal momentum balance is, once again,

$$\frac{\partial u^s}{\partial t} = -\frac{1}{\rho^s} \frac{\partial p^s}{\partial x} + \frac{\partial}{\partial z} \left(\kappa^s \frac{\partial u^s}{\partial z} \right), \quad (3)$$

where superscript s denotes variables in the *seasonal* run. However, the partitioning between the terms is quite different from the *control* run. The variability of upper ocean acceleration is much smaller in the *seasonal* run - the daily standard deviation of $\frac{\partial u^s}{\partial t}$ is 1.16 compared to 2.70 for daily $\frac{\partial u}{\partial t}$ (Table 2). The variability of zonal pressure force is comparable in the two runs; although the standard deviation of stress is only 70% larger in the *control* run, net nonlinearity is 200% larger. Normalised by the variability of acceleration, however, the variability of pressure is twice as large, stress 30% larger and net advection 15% larger in the *seasonal* run. The slowly varying currents in the *seasonal* run arise from the small difference between the (generally positive) stress and (negative) pressure terms, with substantial contribution from nonlinearity.

b. Experiments with Idealized Winds

The response of the EqIO to westerly wind bursts is studied with the help of two experiments (Table 1). The initial stratification of the model ocean is uniform, taken to be the annual mean Levitus temperature and salinity averaged over 10°S-25°N, 30°E-110°E. A spatially uniform, purely zonal wind stress forces the ocean: In the 20-day burst run, it increases smoothly to 0.1 N m⁻² in 10 days, and drops to zero in the next 10 days. In the 60-day burst run, τ_x increases to 0.04 N m⁻² in 10 days, remains constant for 40 days and drops to zero by day 60. The 60-day experiment can be considered an idealisation of fall, when the ocean is forced for about two months by westerly winds; often τ_x strengthens and relaxes abruptly (0.1 N m⁻² change in a week). Note that upper ocean ZPG is generally weak at the start of the fall westerly winds (Figure 9).

The initial response of the upper ocean to the 20-day burst is an accelerating eastward equatorial jet (Figure 10a). First and second baroclinic mode upwelling Kelvin waves and downwelling Rossby waves are generated at the boundaries to satisfy the no-volume-flux condition. The n=1 Kelvin wave propagates east at about 2.4 m s⁻¹, reaching the eastern boundary on day 30; it lowers sea level, counteracting the elevation due to wind forced equatorial convergence. The n=1 Rossby wave moves west at 0.8 m s⁻¹. The westward pressure force associated with these waves (Figure 10c) arrests the acceleration of the eastward jet (Philander and Pacanowski 1980). (Surface dynamic height gradient selectively depicts the n=1 mode, as discussed before). The boundary-generated Kelvin and Rossby waves give rise to westward u at almost all longitudes in the upper ocean by day 60. Upwelling Rossby waves, generated by reflection of upwelling

Kelvin waves at the eastern boundary starting at day 30, are associated with eastward pressure force (Figure 10c). In the subsurface ocean, westward u (Figure 10b) is decelerated by ZPG associated with an $n=2$ Rossby wave moving west at about 0.5 m s^{-1} (Figure 10d). Comparison with term balances suggests that upper (subsurface) ocean ZPG estimated from dynamic height gradient has an error of upto 10% (30%).

Second and higher baroclinic modes are clearer in longitude-depth sections (Figure 11). On day 20, the eastward jet dominates the flow in the upper 100 m or so; the $n=1$ Kelvin wavefront has arrived just west of the Chagos ridge at 73°E , and the Rossby wavefront at 83°E (Figure 11a). On day 30, the $n=1$ Kelvin wave has reached the eastern boundary (see Figure 10c), and the $n=2$ Kelvin wave is west of 65°E (Figure 11b and 10d). 40 days later, the $n=1$ and $n=2$ direct Rossby waves are west of 73°E ; reflected upwelling Rossby waves, which have higher amplitude than the direct Rossby wave, are associated with eastward subsurface u in the eastern basin (Figure 11c). Snapshots of horizontal currents show the propagation of the reflected Rossby wave, and suggest that it has vertical structure resembling a second baroclinic mode (Figure 11e,f), with a zero-crossing in the upper ocean. The direct Rossby wave is also discernible at sub-thermocline depth, to the west of the reflected wave (Figure 11f). Eventually, $n=2$ and higher baroclinic mode Rossby waves give rise to increasingly surface intensified eastward u (Figure 11d) that effectively moves slowly westward at about $0.3\text{-}0.4 \text{ m s}^{-1}$, as seen in Figure 10a and 10d. There is evidence of higher baroclinic mode Kelvin waves near the western boundary. However, these are attenuated by mid-basin (Figure 11b; Figure 10c,d). Generation of the $n=2$ Kelvin wave does not appear to be sustained for long, possibly due to upwelling, which rapidly reduces the directly wind forced eastward volume flux near the western boundary.

The evolution of equatorial u in the 60-day burst experiment is qualitatively similar. It takes about a month longer to replace the eastward jet by westward flow in the 60-day run (Figure 12) than in the 20-day run (not shown). Momentum balance suggests that upper ocean westward u cannot appear until westerly wind stress is switched off (Philander and Pacanowski 1980). Upper ocean zonal pressure force is westward in the first 80 or 90 days in both 60-day (Figure 12a) and 20-day runs; subsequently it is weakly eastward. As in the *control* run, the upper ocean zonal acceleration is mainly due to stress and pressure; nonlinearity strengthens the jet and prolongs eastward flow by several days (Philander and Pacanowski 1980) (Figure 12b,c). The pressure force in the subsurface ocean has the same sign as in the upper layer until day 50 or 60, after which it is eastward for just over two months (Figure 12d). The adjustment of the upper 200 m of the ocean to a single westerly burst is essentially complete (i.e. $\frac{\partial u}{\partial t}$ becomes small) in six or seven months in both experiments.

Once a zonal pressure gradient is set up by a westerly wind burst, its relaxation time can be longer than the burst duration. An important finding is that the variability of ZPG in the upper 200 m has an intrinsic 80-100 day time scale. The burst experiments suggest that the pressure time scale is independent of the forcing duration. We propose that this internal time scale explains the absence of a spectral valley between the intraseasonal and semiannual variability of ZPG and u in the eastern EqIO (Figure 8). Our finding is consistent with the presence of a statistically significant 90 day peak in observed sea level in the eastern EqIO (Qiu et al. 1999; Han et al. 2001). Previous studies using ocean models forced by NCEP reanalysis winds show that the 90 day variability in sea level and zonal current is associated with equatorial waves (Han et al. 2001; Han 2005). NCEP zonal wind stress has a 90 day spectral peak, leading to the suggestion that

the strong 90 day ocean response in the model is mainly due to resonant excitation of $n=2$ waves, as well as to directly wind forced variability. (The possibility of resonance on semiannual scale was proposed by Jensen (1993) and others (SM)). However, QuikSCAT zonal wind stress does not have a 90 day peak. Therefore it is not likely that the 90 day time scale of ocean variability is due to 90 day wind forcing. The 90 day scale is intrinsic to equatorial Indian Ocean adjustment to westerly τ_x . Secondly, the burst experiments suggest that upward phase propagation in the subsurface ocean (not shown) is associated with baroclinic Rossby waves generated at the eastern boundary; boundary waves are also responsible for the qualitatively different evolution of pressure force in the upper and subsurface ocean (see Figure 9).

The burst runs show that easterly wind is not necessary for the generation of transient upper ocean westward flow or eastward undercurrents, in agreement with previous work (SM; Cane 1980). Eastward subsurface u , appearing in the eastern EqIO weeks after the end of a westerly wind burst, can subsequently lie beneath westward u (Figures 11, 12). An EUC is therefore expected two times a year (Bubnov 1994; Reppin et al. 1999), following sustained westerly wind in October-December and April-May. An estimate of the contribution of easterly τ_x winds to EUC transport comes from the “equatorial $\tau_x=0$ experiment” (Table 1): Zonal wind stress is prescribed to be zero within four degrees of the equator from 15 December 2001 to 15 April 2002 (Figure 13a); there are two episodes of significant easterly τ_x in this period (see Figure 6). The 15 February - 15 April 2002 EUC transport between 2°S - 2°N and 60-200 m depth, averaged over 60°E - 90°E , is about 15.5 Sverdrup ($10^6 \text{ m}^3 \text{ s}^{-1}$; Sv) in the control run and 12 Sv in the experiment (Figure 13b); EUC speed is 20-30% higher in the control run (Figure 13c,d). Although easterly winds are not essential to generate EUC in the Indian Ocean, they can enhance

subsurface eastward transport.

The relatively short time scale of adjustment of the equatorial Indian Ocean is associated with basin size. Giese and Harrison (1990) forced a model of the Pacific with a stationary 20-day westerly wind burst with zonal and meridional extent 20 degrees and 6 degrees. A succession of free first, second and higher mode baroclinic Kelvin waves generated by the westerly wind burst are seen east of the forcing region. Due to the large zonal extent of the Pacific basin, $n=1$, 2 and 3 Kelvin wave packets are well separated in longitude by day 60. These waves reflect as Rossby waves at the eastern boundary; however, the Rossby waves give weak westward u even with a 2.0 N m^{-2} wind burst, except near the eastern boundary. The Rossby waves in our 20-day burst experiment carry a much larger u signal to the central and western Indian Ocean because of the small basin size and the larger fetch of our zonally uniform wind burst. We note that free Kelvin waves forced in mid-basin by westerly bursts are apparent in the Indian Ocean as well. For example, the intraseasonal eastward propagating u signals in August-November 2002 (Figure 6,7b,c) appear to be associated with $n=1$ and $n=2$ free downwelling Kelvin waves forced by zonally nonuniform τ_x (Figure 7c).

5. Conclusions

Accurate, high frequency QuikSCAT surface wind stress is used to force an Indian Ocean general circulation model. Comparison with satellite sea level and new *in situ* observations from the eastern EqIO shows that the model simulation of equatorial upper ocean currents, thermocline depth, and zonal pressure gradient is fairly accurate on intraseasonal to interannual scale. When the

model is forced by daily NCEP winds, intraseasonal variability of model currents and subsurface temperature have large differences with observations. The realism of the QuikSCAT simulation is due to the quality of the satellite wind product. Most of the intraseasonal variability in the equatorial waveguide is directly forced by variability of the wind. A part of the intraseasonal variability near the western boundary and in the eastern Indian Ocean arises from dynamic instability of seasonal flows. The QuikSCAT simulation captures observed intraseasonal variability in spite of the presence of instability. An important implication is that equatorial Indian Ocean circulation in the open ocean is a deterministic response to wind forcing. Away from western boundaries, instabilities cannot grow to large amplitude because their energy is rapidly removed by propagating waves (Philander 1990; Sengupta et al. 2001).

Climatologies suggest that zonal windspeed increases with distance from the Indian Ocean equator; the line of zero zonal wind lies close to the equator at most longitudes, particularly in summer and winter (Saji and Goswami 1996). The NCEP reanalysis winds are reasonably accurate in the Bay of Bengal or Arabian Sea, but intraseasonal variability of zonal wind has a weak bias in the EqIO. Westerly wind bursts, associated with atmospheric convection in the central and eastern EqIO, are weak in the reanalysis product (Goswami and Sengupta 2003). The high resolution QuikSCAT zonal wind consists of a series of intraseasonal westerly wind bursts, most intense in the central and eastern EqIO. Between July 1999 and December 2003, strong westerly bursts are absent only in the winter of 2001-2002 and 2002-2003, and in June-July 2003 (Figure 6). The zonal scale of the wind bursts is comparable to the size of the basin except in summer, when they occur in the east. Zonal wind stress has distinct variability on semiannual and intraseasonal (10-30 day, 30-60 day) time scales. Zonal upper ocean current at the equator also

has two distinct, directly wind forced, spectral peaks at semiannual and 30-60 day periods. The spring Wyrtki jet consists of a single intraseasonal event with a lifetime of 30-50 days at 90°E. The fall Wyrtki jet is longer lived, but is modulated on intraseasonal time scales, or actually consists of two or more intraseasonal jets. There are one or two intraseasonal eastward jets each summer in the eastern EqIO (the monsoon jets), but not in winter. Subsurface u is mainly semiannual (Gent et al. 1983; Masumoto et al. 2005), with some intraseasonal variability forced by zonal pressure force.

Eastward equatorial jets accelerate within days of the onset of westerly winds. If the jets have a lifetime of 20-50 days, as the direct observations show, they must be rapidly decelerated. Experiments with 20-day and 60-day zonally uniform westerly wind burst forcing suggest that westward pressure force associated with Kelvin and Rossby boundary waves decelerates eastward jets within days of the weakening of a burst. The simulation suggests that large, abrupt pressure changes are due to Kelvin waves generated in mid-basin by zonally nonuniform wind bursts. Westerly bursts in the central EqIO create westward pressure force in the east in about 15 days. The relatively small basin size ensures that westward pressure force propagates rapidly to the central EqIO. Apart from the semiannual and intraseasonal peaks, upper ocean zonal pressure gradient and currents have an 80-100 day variability (Figure 8), which is absent from QuikSCAT zonal wind. The wind burst experiments confirm that the 90 day response is independent of the time scale of forcing. It arises from the natural time scale of evolution of zonal pressure force associated with boundary waves. In other words, the 90 day time scale is intrinsic to equatorial adjustment of the Indian Ocean to intraseasonal westerly winds.

In all generality, the evolution of equatorial circulation is a nonlinear problem because the

pressure force depends on the zonal flow. However, the strongest nonlinearity in the upper ocean zonal momentum balance comes from the vertical advection term $w \frac{\partial u}{\partial z}$ (Figure 9, Table 2). Fluctuations of vertical velocity w and vertical shear of u are both more responsive to fluctuating stress than to zonal pressure force. Although nonlinearity is a significant component of the dynamical balance, it does not dominate the evolution of u (Figure 9b) (Sengupta et al. 2001). There is an eastward equatorial undercurrent in July-September each year, in addition to the spring undercurrent. Neither the westward current in the upper ocean nor the subsequent eastward flow (the observed early spring and late summer EUC) requires easterly winds; they are mainly generated by variable westerly winds via wave-mediated equatorial adjustment. For example, the contribution of December 2001 - March 2002 easterly winds to the transport of the February-April 2002 eastward undercurrent is only 20%. In general, the response to wind bursts is determined by wind stress and zonal pressure force, with substantial contribution from nonlinearity. The quantitative dynamical balance is rather different in an experiment where the model is forced by smoothed seasonally varying winds with no wind bursts. The current in the *seasonal* run evolves slowly in response mainly to the difference between the seasonal stress and seasonal pressure force, which have comparable magnitudes (Table 2) but differ in phase. The satellite and *in situ* observations show that continual intraseasonal changes in stress and pressure do not permit the upper equatorial Indian Ocean such a slow approach towards equilibrium. Our analysis of zonal currents in the upper 200 m of the ocean, based on new wind observations, focuses on the simplest features of the dynamics of intraseasonal and seasonal variability. We have not examined interannual variability because the QuikSCAT wind record is not long, nor have we addressed more involved questions such as the possibility of rectification, or of resonance. The present results might provide a basis

for further investigation of these and related questions.

Acknowledgement We acknowledge the Department of Ocean Development for continued support. Discussions with V. S. N. Murty and Y. Masumoto about the observations, and D. S. Anitha's work on validation of QuikSCAT and NCEP winds was very useful in the course of this work. We thank Y. Masumoto for the ADCP data. The QuikSCAT wind data were obtained from ftp://podaac.jpl.nasa.gov/pub/ocean_wind/quikscat of Physical Oceanography Distributed Active Archive Center (PO.DAAC), NASA Jet Propulsion Laboratory, Pasadena, U.S.A. The TOPEX/Poseidon data was obtained from Centre for Space Research, University of Texas at Austin (<http://www.csr.utexas.edu/sst/gpdata.html>). The Jason-1 altimeter data was obtained from AVISO, France (http://www.aviso.oceanobs.com/html/donnees/produits/msla_uk.html).

References

- Anderson, D. L. T. and D. J. Carrington, 1993: Modeling interannual variability in the Indian Ocean using momentum fluxes from the operational weather analysis of the United Kingdom Meteorological Office and European Centre for Medium Range Weather Forecasts. *J. Geophys. Res.*, **98**, 12483–12499.
- Bubnov, V. A., 1994: Climatic zonal pressure gradient in the equatorial zone of the Indian ocean. *Oceanology*, **33**, 414–420.
- Cane, M., 1980: On the dynamics of equatorial currents, with application to the Indian Ocean. *Deep-Sea Res.*, **27A**, 525–544.
- Chatfield, C., 1975: *The analysis of time series: Theory and practice*. Chapman and Hall, London, 263 pp.
- Chatterji, P. and B. N. Goswami, 2004: Structure, Genesis and Scale Selection of the Tropical Quasi-Biweekly mode. *Quart. J. Roy. Meteor. Soc.*, **130**, 1171–1194.
- Chelton, D. B., S. K. Esbensen, M. G. Schlax, N. Thum, M. H. Freilich, F. J. Wentz, C. L. Gentemann, M. J. McPhaden, and P. S. Schopf, 2001: Observations of coupling between surface wind stress and sea surface temperature in the eastern Tropical Pacific. *J. Climate*, **14**, 1479–1498.
- Eriksen, C. C., 1979: An equatorial transect of the Indian Ocean. *J. Mar. Res.*, **37**, 215–232.

- Fu, L. L., E. J. Christensen, C. A. Yamarone, M. Lefebvre, Y. Menard, M. Dorrer, and P. Escudier, 1994: TOPEX/POSEIDON mission overview. *J. Geophys. Res.*, **99**, 24,369–24,382.
- Fu, L. L., D. Stammer, R. Leben, and D. B. Chelton, 2003a: Improved spatial resolution of ocean surface topography from the T/P-Jason-1 altimeter mission. *Eos, AGU*, **84**, 247–248.
- Fu, X., B. Wang, T. Li, and J. McCreary, 2003b: Coupling between northward propagating, intraseasonal oscillations and sea-surface temperature in the Indian Ocean. *J. Atmos. Sci.*, **60**, 1733–1753.
- Gent, P. R., K. O’Neill, and M. A. Cane, 1983: A model of the semiannual oscillation in the Equatorial Indian Ocean. *J. Phys. Oceanogr.*, **13**, 2148–2160.
- Giese, B. S. and D. E. Harrison, 1990: Aspect of the Kelvin wave response to episodic wind forcing. *J. Geophys. Res.*, **95**, 7289–7312.
- Godfrey, J. S., G. Johnson, M. J. McPhaden, G. Reverdin, and S. E. Wiffels, 2001: *Ocean Circulation and Climate: Observing and Modeling the Global Ocean*, Academic Press, The Tropical Ocean Circulation. 215–246.
- Goswami, B. N., 2005: *Intraseasonal Variability of the Atmosphere-Ocean Climate System*, South Asian Monsoon, W. K. M. Lau and D. E. Waliser, Eds., Praxis Publishing. 19–61.
- Goswami, B. N. and D. Sengupta, 2003: A Note on the Deficiency of NCEP/NCAR Reanalysis Surface Winds over the Equatorial Indian Ocean. *J. Geophys. Res.*, **108**, doi:10.1029/2002JC001497.

- Grodsky, S. A., J. Carton, and R. Murtugudde, 2001: Anomalous surface currents in the tropical Indian Ocean. *Geophys. Res. Lett.*, **28**, 4207–4210.
- Han, W., 2005: Origins and dynamics of the 90-day and 30-60 day variations in the equatorial Indian Ocean. *J. Phys. Oceanogr.*, **35**, 708–728.
- Han, W., D. M. Lawrence, and P. J. Webster, 2001: Dynamical response of equatorial Indian Ocean to intraseasonal winds: zonal flow. *Geophys. Res. Lett.*, **28**, 4215–4218.
- Han, W., J. P. McCreary, J. D. L. T. Anderson, and A. J. Mariano, 1999: On the dynamics of the eastward surface jets in the equatorial Indian Ocean. *J. Phys. Oceanogr.*, **29**, 2191–2209.
- Han, W., P. J. Webster, R. Lukas, P. Hacker, and A. Hu, 2004: Impact of atmospheric intraseasonal variability in the Indian Ocean: low-frequency rectification in equatorial surface current and transport. *J. Phys. Oceanogr.*, **34**, 1350–1372.
- Jensen, T. G., 1993: Equatorial variability and resonance in a wind-driven Indian Ocean Model. *J. Geophys. Res.*, **98**, 22533–22552.
- Kalnay, E., M. Kanamitsu, R. Kistler, W. Collins, D. Deaven, L. Gandin, M. Iredell, S. Saha, G. White, J. Woollen, Y. Zhu, A. Leetmaa, B. Reynolds, M. Chelliah, W. Ebisuzaki, W. Higgins, J. Janowiak, K. C. Mo, C. Ropelewski, R. J. J. Wang, and D. Joseph, 1996: The NCEP/NCAR 40-year reanalysis project. *Bull. Amer. Meteor. Soc.*, **77**, 437–471.
- Knox, R., 1976: On a long series of measurements of Indian Ocean equatorial currents near Addu Atoll. *Deep-Sea Res.*, **23**, 211–221.

- Kuroda, Y., 2002: TRITON: Present Status and Future Plan. Technical Report JAMSTEC Tech. Rept. TOCS No. 5, Japan Marine Science and Technology Center, Yokosuka, Japan.
- Le Blanc, J.-L. and J.-P. Boulanger, 2001: Propagation and reflection of long equatorial waves in the Indian Ocean from TOPEX/POSEIDON data during the 1993-1998 period. *Climate Dyn.*, **17**, 547–557.
- Levitus, S., 1982: *Climatological atlas of the world ocean*. NOAA Prof. Pap, U. S. Govt. Print. Off., Washington, D.C.
- Liu, W. T., 2002: Progress in Scatterometer Application. *J. Oceanogr.*, **58**, 121–136.
- Loschnigg, J. and P. J. Webster, 2000: A coupled ocean-atmosphere system of SST modulation for the Indian Ocean. *J. Climate*, **13**, 3342–3360.
- Luyten, J. R. and D. H. Roemmich, 1982: Equatorial currents at semiannual period in the Indian Ocean. *J. Phys. Oceanogr.*, **12**, 406–413.
- Masson, S., J.-P. Boulanger, C. Menkes, P. Delecluse, and T. Yamagata, 2004: Impact of salinity on the 1997 Indian Ocean dipole event in a numerical experiment. *J. Geophys. Res.*, **109**, doi:10.1029/2003JC001807.
- Masumoto, Y., H. Hase, Y. Kuroda, H. Matsuura, and K. Takeuchi, 2005: Intraseasonal variability in the upper layer currents observed in the eastern equatorial Indian Ocean. *Geophys. Res. Lett.*, **32**, doi:10.1029/2004GL021896.
- McCreary, J. P., P. k. Kundu, and R. L. Molinari, 1993: A numerical investigation of dynamics,

- thermodynamics and mixed-layer processes in the Indian Ocean. *Prog. Oceanogr.*, **31**, 181–244.
- McPhaden, M. J., 1982: Variability in the central equatorial Indian Ocean Part I: Ocean dynamics. *J. Mar. Res.*, **40**, 157–176.
- Moore, D. W. and J. P. McCreary, 1990: Excitation of intermediate frequency equatorial waves at a western ocean boundary: With application to observations from the western Indian Ocean. *J. Geophys. Res.*, **95**, 5219–5231.
- Murtugudde, R., J. McCreary, and A. Busalacchi, 2000: Oceanic processes associated with anomalous events in the Indian Ocean with relevance to 1997-98. *J. Geophys. Res.*, **105**, 3295–3306.
- Murtugudde, R., S. Signorini, J. Christian, A. Busalacchi, C. McClain, and J. Picaut, 1999: Ocean color variability of the tropical Indo-Pacific basin observed by SeaWiFS during 1997 98. *J. Geophys. Res.*, **104**, 18351–18366.
- Murty, V. S. N., A. Suryanarayana, M. Sarma, V. Tilvi, V. Fernando, G. Nampoothiri, A. Sardar, D. Gracias, and S. Khalap, 2002: First results of Indian current meter moorings along the equator: Vertical current structure variability at equator, 93E during February-December 2000. *Proc. 6th Pan Ocean Remote Sensing Conference, PORSEC 2002, Bali, Indonesia*, 1, 25–28.
- Pacanowski, R. C., 1996: *MOM2 Version 2.0(beta): Documentation, user's guide and reference manual*. GFDL Ocean Technical Report 3.2. Geophysical Fluid Dynamics Laboratory, Princeton NJ.

- Pacanowski, R. C. and S. G. H. Philander, 1981: Parameterization of vertical mixing in numerical models of tropical oceans. *J. Phys. Oceanogr.*, **11**, 1443–1451.
- Pegion, P. J., M. A. Bourassa, D. M. Legler, and J. J. O’Brien, 2000: Objectively-derived daily “winds” from satellite scatterometer data. *Mon. Wea. Rev.*, **128**, 3150–3168.
- Philander, S. G. H., 1990: *El Niño, La Niña and the Southern Oscillation*. Academic Press, San Deigo, 293 pp.
- Philander, S. G. H. and R. C. Pacanowski, 1980: The generation of equatorial currents. *J. Geophys. Res.*, **85**, 1123–1136.
- Qiu, B., M. Mao, and Y. Kashino, 1999: Intraseasonal variability in the Indo-Pacific Throughflow and the regions surrounding the Indonesian Seas. *J. Phys. Oceanogr.*, **29**, 1599–1618.
- Reppin, J., F. Schott, J. Fischer, and D. Quadfasel, 1999: Equatorial currents and transports in the upper central Indian Ocean. *J. Geophys. Res.*, **104**, 15495–15514.
- Reverdin, G., D. L. Cadet, and D. Gutzler, 1986: Interannual displacements of convection and surface circulation over the equatorial Indian Ocean. *Quart. J. Roy. Meteor. Soc.*, **112**, 43–67.
- Saji, N. H. and B. N. Goswami, 1996: An improved linear model of tropical surface wind variability. *Quart. J. Roy. Meteor. Soc.*, **122**, 23–53.
- Saji, N. H., B. N. Goswami, P. N. Vinayachandran, and T. Yamagata, 1999: A dipole mode in the tropical Indian Ocean. *Nature*, **401**, 360–363.

- Saji, N. H., S. P. Xie, H. Hase, Y. Kuroda, Y. Masumoto, M. Nonaka, and H. Sasaki, 2005: Intraseasonal air-sea interactions over the tropical South Indian Ocean: Satellite and in-situ observations. *J. Climate*, submitted.
- Schiller, A. and J. S. Godfrey, 2001: Indian Ocean intraseasonal variability in an Ocean General Circulation Model. *J. Climate*, **16**, 21–31.
- Schiller, A., J. S. Godfrey, P. C. McIntosh, G. Meyers, and R. Fiedler, 2000: Interannual Dynamics and Thermodynamics of the Indo-Pacific Oceans. *J. Phys. Oceanogr.*, **30**, 987–1012.
- Schott, F., M. Dengler, and R. Schoenefeldt, 2002: The shallow overturning circulation of the Indian Ocean. *Prog. Oceanogr.*, **53**, 57–103.
- Schott, F. and J. P. McCreary, 2001: The monsoon circulation of the Indian Ocean. *Prog. Oceanogr.*, **51**, 1–123.
- Schott, F., J. Reppin, J. Fischer, and D. Quadfasel, 1994: Currents and transports of the monsoon current south of Sri Lanka. *J. Geophys. Res.*, **99**, 25127–25141.
- Senan, R., D. Sengupta, and B. N. Goswami, 2003: Intraseasonal “monsoon jets” in the equatorial Indian Ocean. *Geophys. Res. Lett.*, **30**, doi:10.1029/2003GL017583.
- Sengupta, D., R. Senan, and B. N. Goswami, 2001: Origin of Intraseasonal variability of circulation in the tropical central Indian Ocean. *Geophys. Res. Lett.*, **28**, 1267–1270.
- Sengupta, D., R. Senan, V. S. N. Murty, and V. Fernando, 2004: A biweekly mode in the equatorial Indian Ocean. *J. Geophys. Res.*, **109**, doi:10.1029/2004JC002329.

- Shenoi, S. S. C., P. K. Saji, and A. M. Almeida, 1999: Near-surface circulation and kinetic energy in the tropical Indian Ocean derived from Lagrangian drifters. *J. Mar. Res.*, **57**, 885–907.
- Vecchi, G. A. and D. E. Harrison, 2002: Monsoon breaks and subseasonal sea surface temperature variability in the Bay of Bengal. *J. Climate*, **15**, 1485–1493.
- Vinayachandran, P. N., S. R. Shetye, D. Sengupta, and S. Gadgil, 1996: Forcing mechanisms of the Bay of Bengal circulation. *Curr. Sci.*, **71**, 753–763.
- Waliser, D. E., 2005: *Intraseasonal Variability*, The Global Monsoon System: Research and Forecast, C. -P. Chang, B. Wang, N. G. Lau, Eds., WMO Technical Document No. 1266. 403–439.
- Waliser, D. E., R. Murtugudde, and L. Lucas, 2004: Indo-Pacific Ocean Response to Atmospheric Intraseasonal Variability. Part II: Boreal Summer and the Intraseasonal Oscillation. *J. Geophys. Res.*, **109**, doi:10.1029/2003JC002002.
- Webster, P. J., A. M. Moore, J. P. Loschnigg, and R. R. Leben, 1999: The great Indian Ocean warming of 1997-98: Evidence of coupled oceanic-atmospheric instabilities. *Nature*, **401**, 356–360.
- Webster, P. J., T. Palmer, M. Yanai, V. Magana, J. Shukla, and A. Yasunari, 1998: Monsoons: Processes, predictability and the prospects for prediction. *J. Geophys. Res.*, **103**, 14451–14510.
- Wyrtki, K., 1973: An equatorial jet in the Indian Ocean. *Science*, **181**, 262–264.

Zheng, Y., D. E. Waliser, W. Stern, and C. Jones, 2004: The role of coupled sea surface temperatures in the simulation of the tropical intraseasonal oscillation. *J. Climate*, **17**, 4109–4134.

List of Figures

- 1 Evolution of zonal wind stress, zonal current and $d20$ at 1.6°S , 90°E from TRITON data and QuikSCAT simulation, 2002-2003. (a) Three-day τ_x (10^{-1} N m^{-2}), (b) five-day u (m s^{-1}) at 10 m, and (c) five-day 20°C isotherm depth (m). 44
- 2 Surface zonal pressure gradient averaged between $60\text{-}95^{\circ}\text{E}$, $2^{\circ}\text{S}\text{-}2^{\circ}\text{N}$ estimated from satellite sea surface height (bold), 1997-2003, and from the *control* run (thin), July 1999 - December 2003. The observations are from the TOPEX (January 1997 - May 2002) and Jason-1 (June 2002 to December 2003) altimeters. 45
- 3 Time evolution of five-day u (m s^{-1}) in the upper 400 m at 0° , 90°E from the (a) *control* run, and (b) JAMSTEC ADCP observations (data courtesy: Yukio Masumoto). 46
- 4 Daily time series at 0° , 90°E of QuikSCAT (bold) and NCEP (thin) run (a) zonal wind stress (10^{-1} N m^{-2}); (b) 50 m u (m s^{-1}) and (c) potential temperature ($^{\circ}\text{C}$) at 100 m. 47
- 5 Standard deviation of intraseasonal anomalies of (a) τ_x (10^{-1} N m^{-2}) and (b) u (m s^{-1}) at 50 m from the *control* run. 48
- 6 Zonal surface wind stress and current from the *control* (thin) and *seasonal* (bold) runs averaged over $60\text{-}95^{\circ}\text{E}$. (a) QuikSCAT τ_x (10^{-1} N m^{-2}) averaged over $2^{\circ}\text{S}\text{-}2^{\circ}\text{N}$; (b) upper ocean u (m s^{-1}) averaged over 0-120 m, $1^{\circ}\text{S}\text{-}1^{\circ}\text{N}$; (c) subsurface u (m s^{-1}) averaged over 120-200 m, $1^{\circ}\text{S}\text{-}1^{\circ}\text{N}$. Equatorial “undercurrents” are highlighted. 49

7	Time longitude plot of 1°S-1°N averaged (a) 10-day running mean QuikSCAT τ_x (10^{-1} N m ⁻²); (b) daily 0-120 m u (m s ⁻¹) and (c) daily 120-200 m u (m s ⁻¹) from the <i>control</i> run.	50
8	Variance preserving power spectra of July 1999-December 2003 (a) τ_x (bold) and τ_y (thin) averaged over 2°S-2°N, 60-70°E; (b) as in (a), but for 80-95°E; (c) <i>control</i> run u (bold), v (thin) and ZPG (grey) averaged over 0-120 m, 1°S-1°N, 60-70°E; (d) as in (c), but for 80-95°E; (e) <i>control</i> run u (bold) and ZPG (grey) averaged over 120-200 m, 1°S-1°N, 60-70°E; (f) as in (e), but for 80-95° E. Units are arbitrary, but identical for wind stress, velocity and ZPG across all panels. The lines mark 20 and 60 day period.	51
9	Evolution of terms in the zonal momentum equation in the equatorial strip (60-95°E, 1°S-1°N) from the <i>control</i> run. (a) 0-120 m pressure term (grey) and stress (thin); climatology of zonal pressure gradient from Bubnov (1994) is shown by the dots; (b) 0-120 m zonal acceleration (grey) and sum of the pressure and stress terms (thin); (c) 0-120 m vertical (bold) and meridional (thin) advection terms. (d) 120-200 m zonal acceleration (grey), pressure (thin) and stress (bold). Units of all terms are 10^{-7} m s ⁻²	52

10	20-day burst experiment. Time-longitude plot of (a) 0-80 m u (m s^{-1}) and (b) 120-160 m u at the equator; (c) zonal gradient of surface dynamic height (10^{-7} m s^{-2}) with respect to 500 m and (d) same as (c) but for dynamic height at 120 m. The slopes of the lines in (c) denote the phase speeds of the fastest Kelvin (2.4 m s^{-1}) and Rossby (0.8 m s^{-1}) waves, and (d) are consistent with $n=2$ Kelvin and Rossby wave speeds	53
11	Depth-longitude structure of u (m s^{-1}) at the equator from the 20-day burst experiment, on (a) day 20 (b) day 30 (c) day 70 and (d) day 110. Snapshots of horizontal currents, on (e) day 45 at 105 m and (f) day 70 at 300 m.	54
12	Evolution of terms in the momentum equation in the central Indian Ocean ($70\text{-}80^\circ\text{E}$, $1^\circ\text{S}\text{-}1^\circ\text{N}$) from the 60-day burst experiment. (a) 0-120m u (grey), pressure term (bold) and stress (thin); (b) 0-120m zonal acceleration (thin) and sum of pressure and stress terms (bold); (c) 0-120m zonal (grey), meridional (thin) and vertical (bold) advection terms; (d) 120-200m pressure term (bold) and u (grey). Units of all terms are 10^{-7} m s^{-2} ; u is in m s^{-1}	55
13	Zonal wind stress and zonal flow in the <i>control</i> run (grey) and “Equatorial $\tau_x=0$ experiment” (black). (a) $2^\circ\text{S}\text{-}2^\circ\text{N}$, $60\text{-}90^\circ\text{E}$ average τ_x (10^{-1} N m^{-2}) December 2001-July 2002 (b) $2^\circ\text{S}\text{-}2^\circ\text{N}$, $60\text{-}90^\circ\text{E}$ averaged zonal transport (Sv) in the 60-200 m depth range, (c) depth-latitude section of $60\text{-}90^\circ\text{E}$ average u (m s^{-1}), (d) as in (c), but for the “equatorial $\tau_x=0$ experiment”.	56

Table 1: List of Experiments

Name	Forcing Characteristics
<i>Control</i> run	Three-day running mean wind stress derived from 1999-2003 QSCAT winds.
<i>Seasonal</i> run	Seasonal wind stress, i.e, three-day QSCAT winds with all sub-90 day variability removed.
<i>NCEP</i> run	Wind stress derived from daily mean 10m winds from NCEP/NCAR Reanalysis.
<i>20-day burst</i> run	Uniformly stratified ocean forced by a single burst of spatially uniform purely zonal wind stress. Forcing increases smoothly to 0.1 N m^{-2} in 10 days, and drops to zero in the next 10 days.
<i>60-day burst</i> run	Uniformly stratified ocean forced by a single burst of spatially uniform purely zonal wind stress. Forcing increases smoothly to 0.04 N m^{-2} in 10 days, remains constant for the next 40 days and drops to zero in the next 10 days.
<i>Equatorial $\tau_x=0$</i> run	Zonal wind stress within 4 degrees of the equator is prescribed to be zero from 15 December to 15 April 2002

Table 2: Standard deviation of terms in the zonal momentum equation in the upper equatorial Indian Ocean (0-120 m, 60-95°E, 1°S-1°N)

Term	<i>Control run</i>	<i>Seasonal run</i>	<i>Control run</i> (normalised by Acceleration)	<i>Seasonal run</i>
Acceleration	2.61	1.13	1	1
Pressure	1.51	1.40	0.58	1.24
Stress	2.22	1.36	0.85	1.20
Vertical advection	0.90	0.42	0.35	0.37
Meridional advection	0.51	0.21	0.20	0.19
Zonal advection	0.19	0.13	0.07	0.12
Net advection	0.83	0.28	0.32	0.25

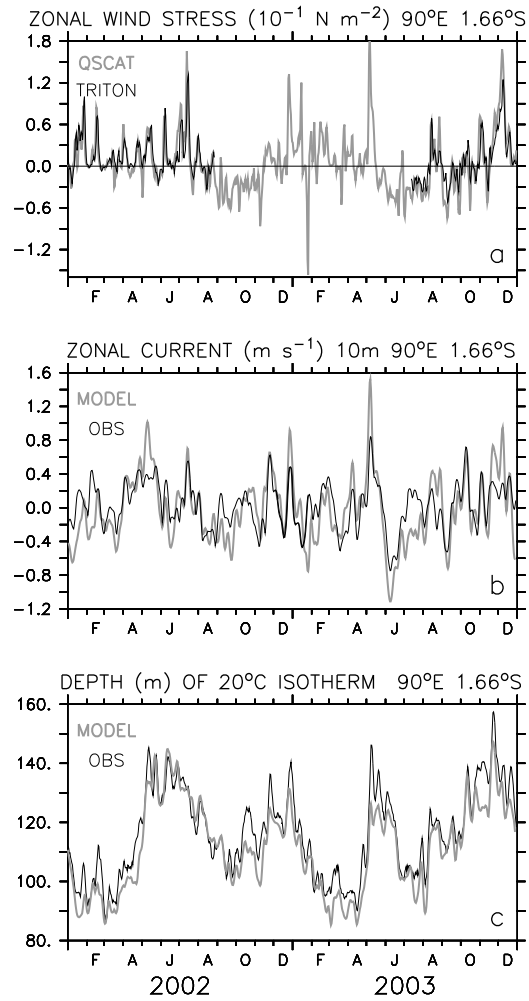


Figure 1: Evolution of zonal wind stress, zonal current and $d20$ at 1.6°S, 90°E from TRITON data and QuikSCAT simulation, 2002-2003. (a) Three-day τ_x (10^{-1} N m^{-2}), (b) five-day u (m s^{-1}) at 10 m, and (c) five-day 20°C isotherm depth (m).

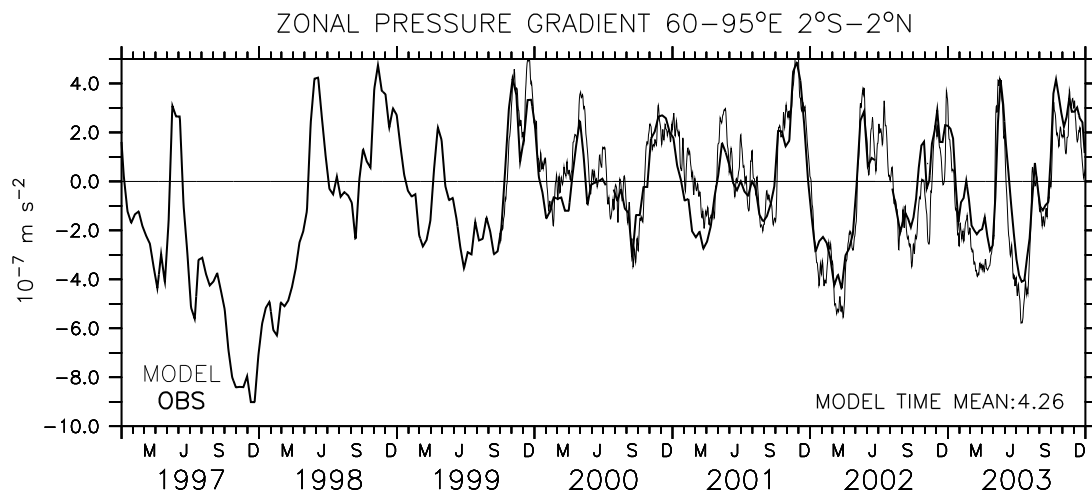


Figure 2: Surface zonal pressure gradient averaged between 60-95°E, 2°S-2°N estimated from satellite sea surface height (bold), 1997-2003, and from the *control* run (thin), July 1999 - December 2003. The observations are from the TOPEX (January 1997 - May 2002) and Jason-1 (June 2002 to December 2003) altimeters.

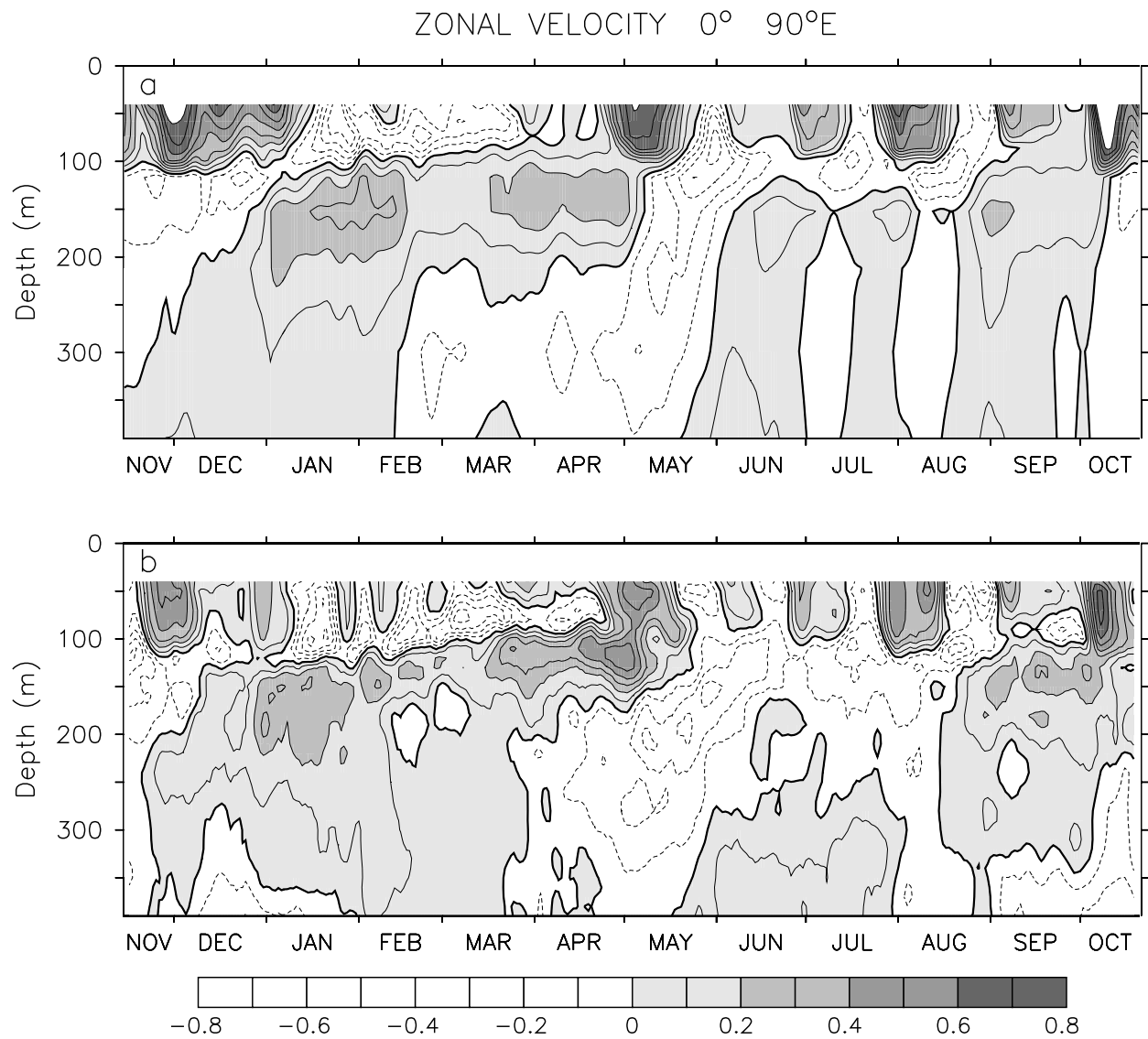


Figure 3: Time evolution of five-day u (m s^{-1}) in the upper 400 m at 0° , 90°E from the (a) *control* run, and (b) JAMSTEC ADCP observations (data courtesy: Yukio Masumoto).

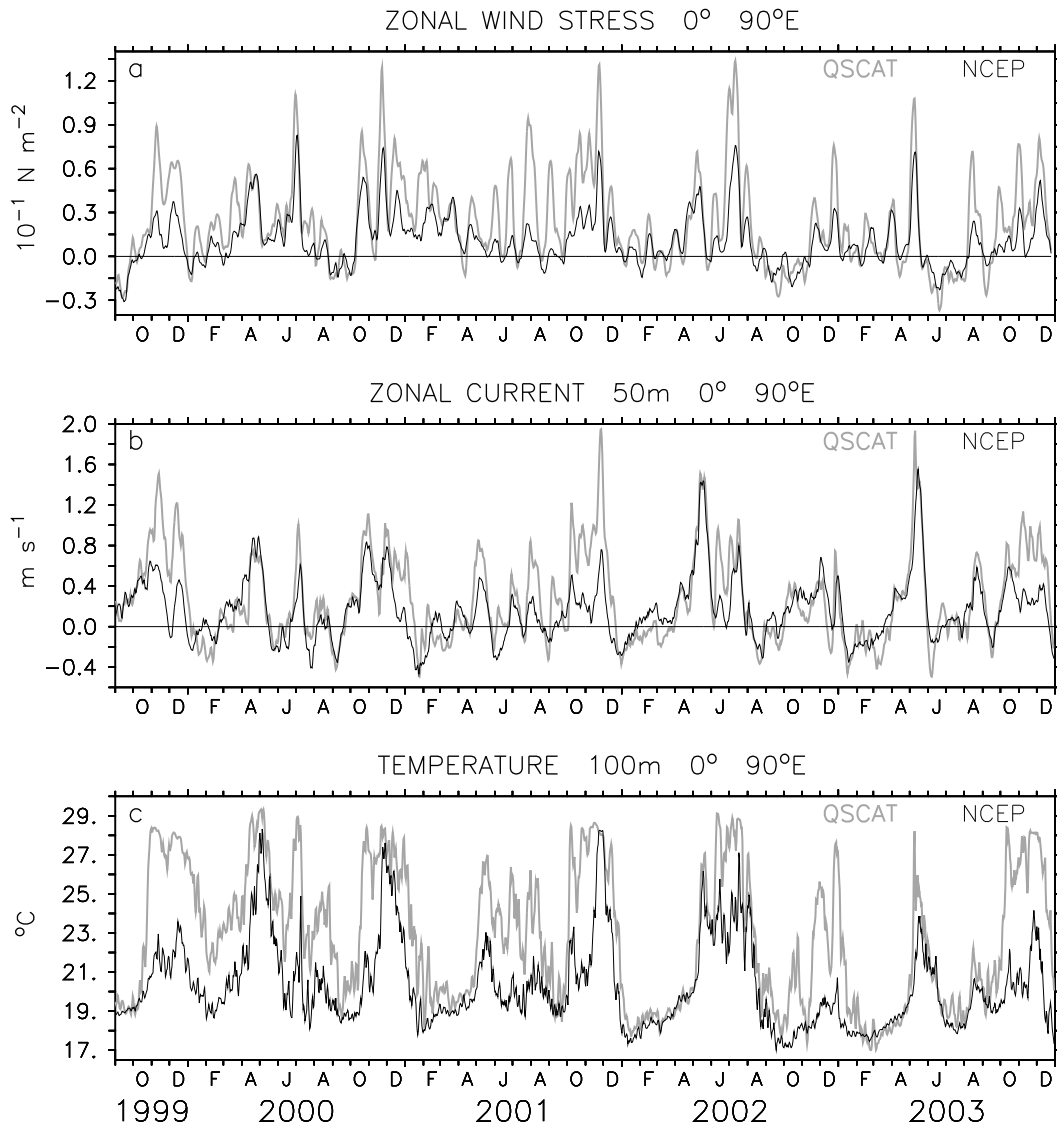


Figure 4: Daily time series at 0°, 90°E of QuikSCAT (bold) and NCEP (thin) run (a) zonal wind stress (10^{-1} N m^{-2}); (b) 50 m u (m s^{-1}) and (c) potential temperature ($^{\circ}\text{C}$) at 100 m.

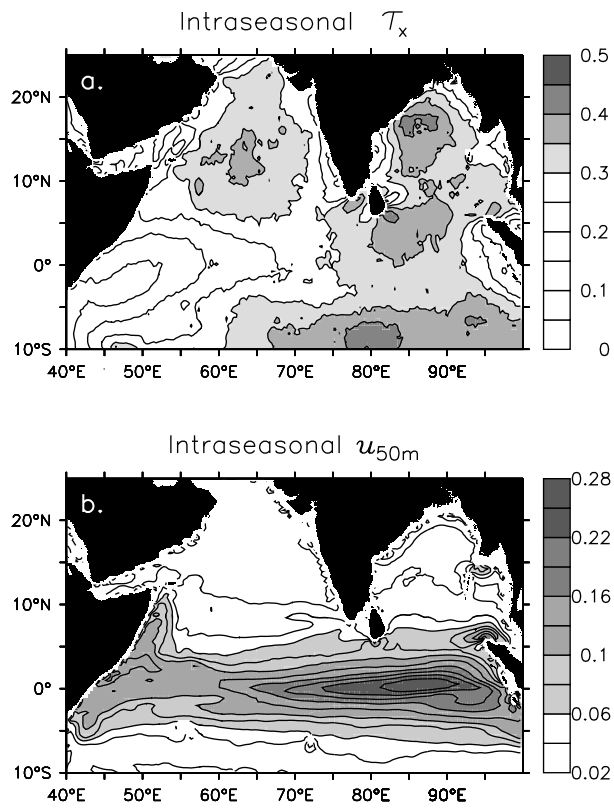


Figure 5: Standard deviation of intraseasonal anomalies of (a) τ_x (10^{-1} N m^{-2}) and (b) u (m s^{-1}) at 50 m from the *control* run.

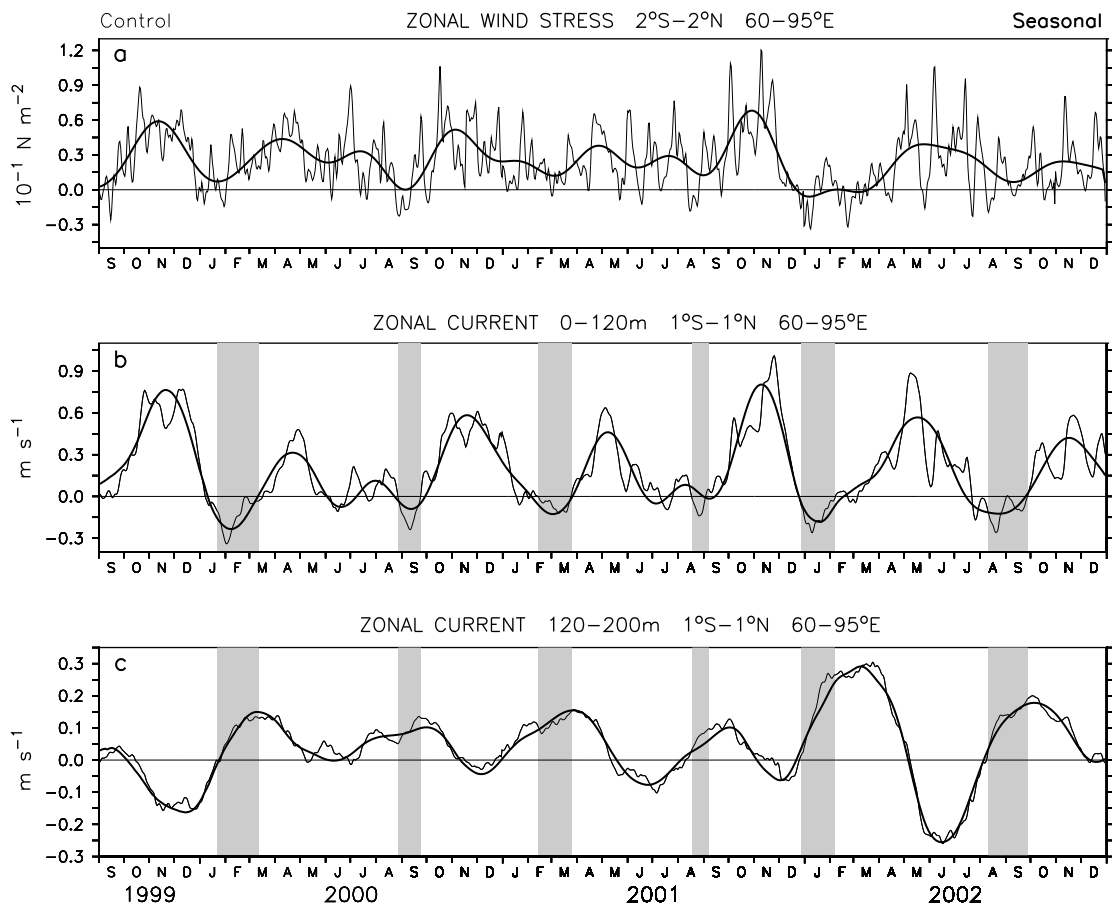


Figure 6: Zonal surface wind stress and current from the *control* (thin) and *seasonal* (bold) runs averaged over 60–95°E. (a) QuikSCAT τ_x (10^{-1} N m^{-2}) averaged over 2°S–2°N; (b) upper ocean u (m s^{-1}) averaged over 0–120 m, 1°S–1°N; (c) subsurface u (m s^{-1}) averaged over 120–200 m, 1°S–1°N. Equatorial “undercurrents” are highlighted.

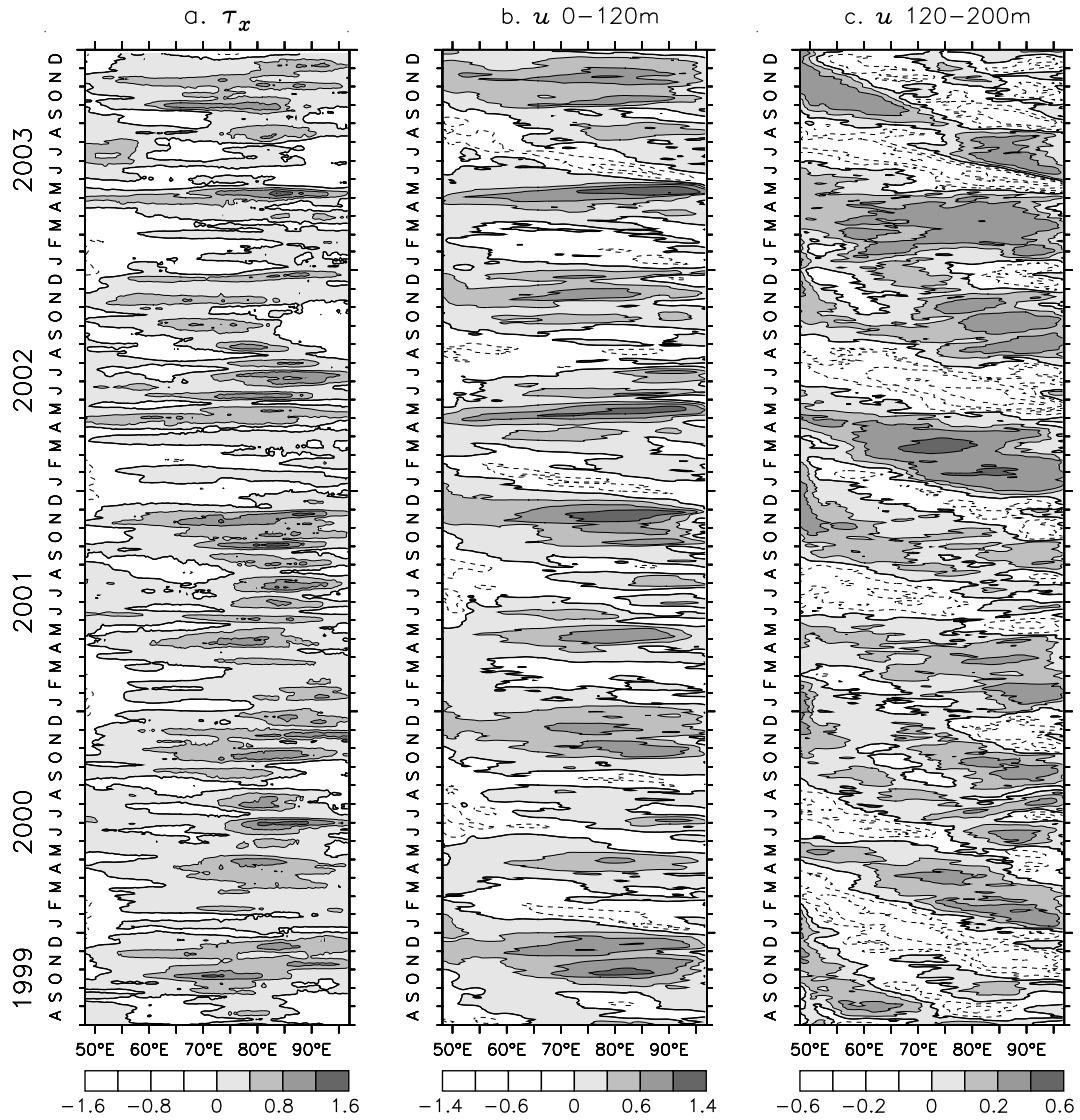


Figure 7: Time longitude plot of 1°S - 1°N averaged (a) 10-day running mean QuikSCAT τ_x (10^{-1} N m^{-2}); (b) daily 0-120 m u (m s^{-1}) and (c) daily 120-200 m u (m s^{-1}) from the *control* run.

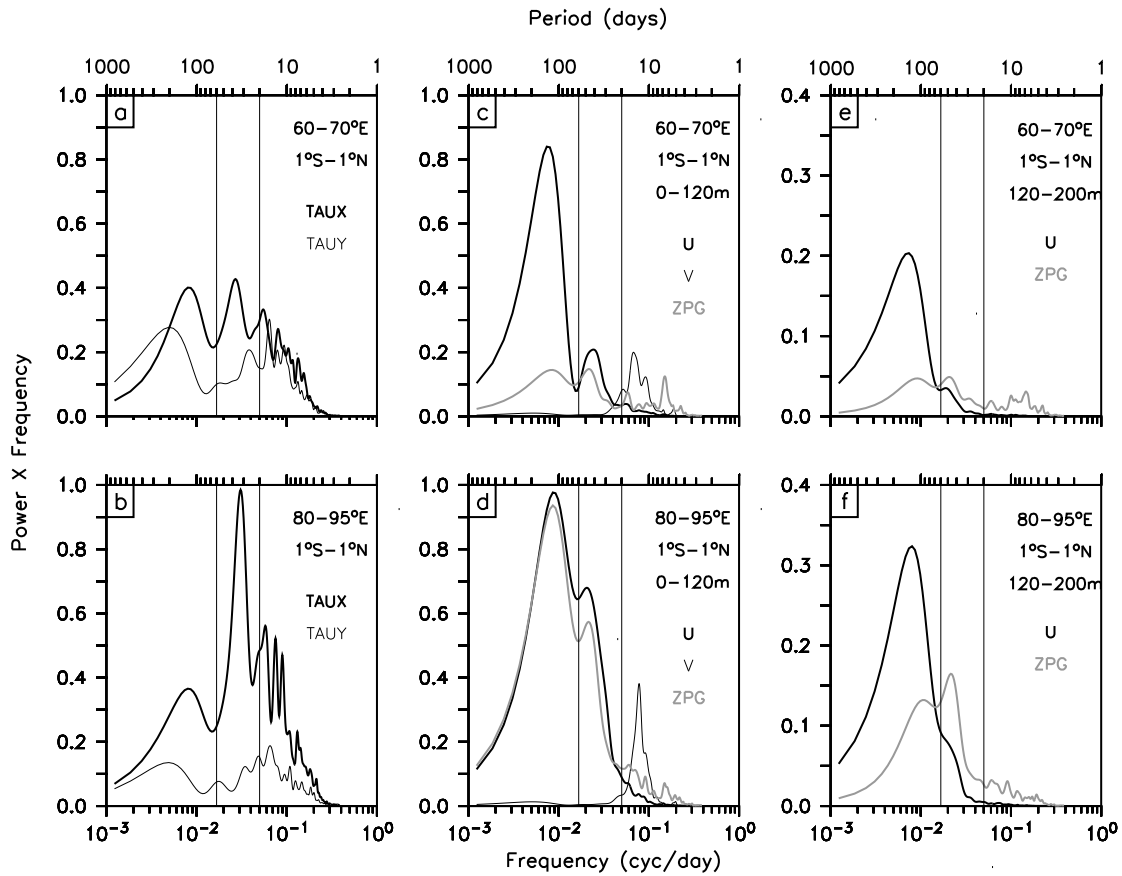


Figure 8: Variance preserving power spectra of July 1999-December 2003 (a) τ_x (bold) and τ_y (thin) averaged over 2°S-2°N, 60-70°E; (b) as in (a), but for 80-95°E; (c) *control* run u (bold), v (thin) and ZPG (grey) averaged over 0-120 m, 1°S-1°N, 60-70°E; (d) as in (c), but for 80-95°E; (e) *control* run u (bold) and ZPG (grey) averaged over 120-200 m, 1°S-1°N, 60-70°E; (f) as in (e), but for 80-95° E. Units are arbitrary, but identical for wind stress, velocity and ZPG across all panels. The lines mark 20 and 60 day period.

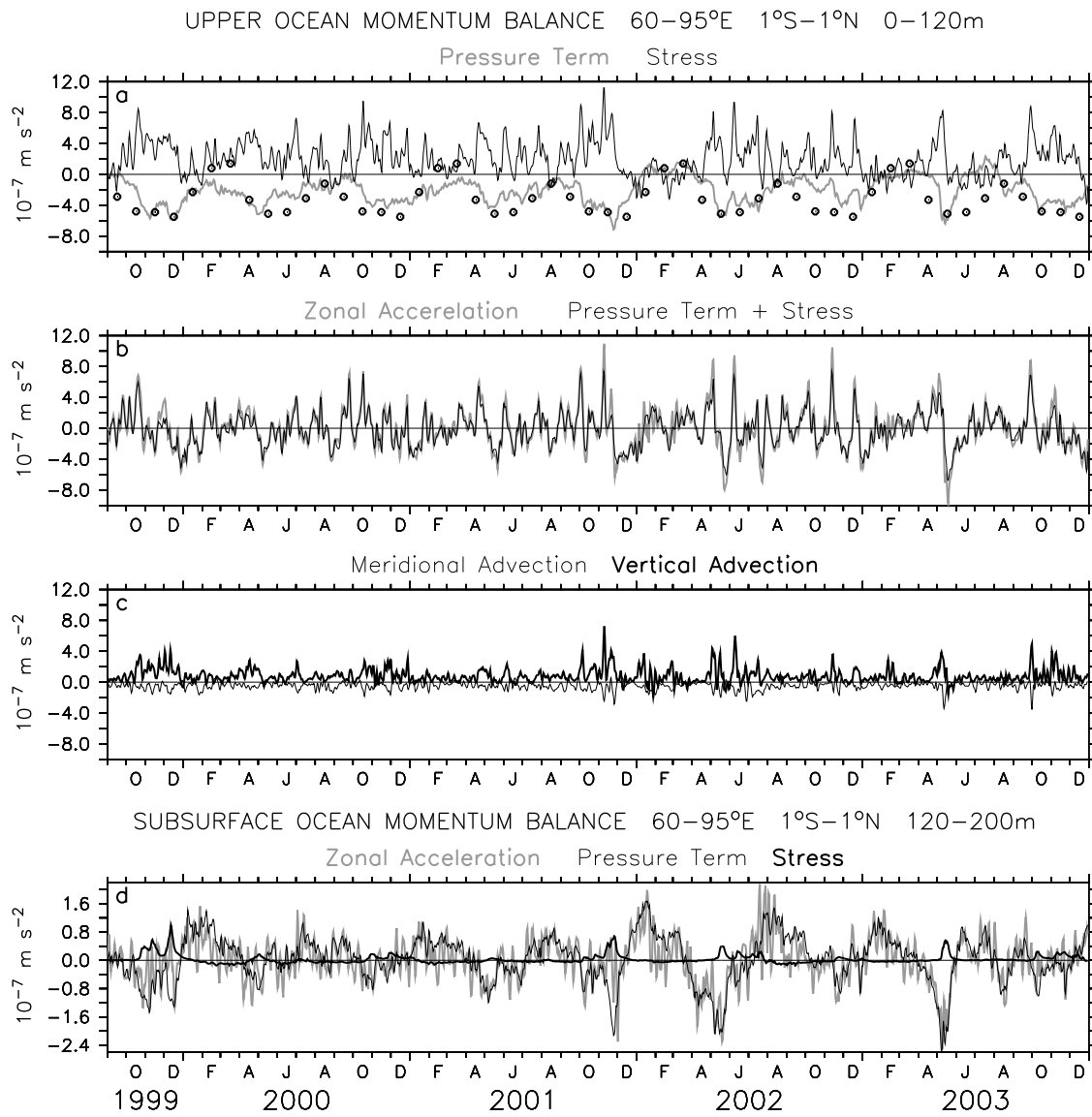


Figure 9: Evolution of terms in the zonal momentum equation in the equatorial strip (60-95°E, 1°S-1°N) from the *control* run. (a) 0-120 m pressure term (grey) and stress (thin); climatology of zonal pressure gradient from Bubnov (1994) is shown by the dots; (b) 0-120 m zonal acceleration (grey) and sum of the pressure and stress terms (thin); (c) 0-120 m vertical (bold) and meridional (thin) advection terms. (d) 120-200 m zonal acceleration (grey), pressure (thin) and stress (bold). Units of all terms are 10^{-7} m s^{-2} .

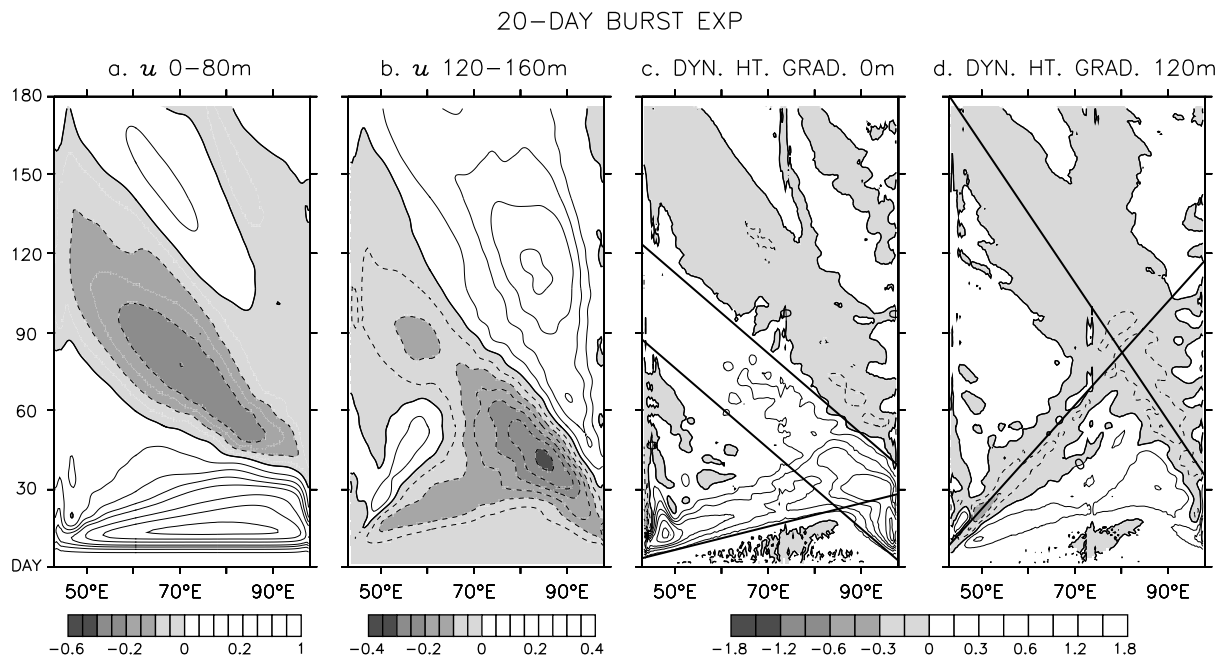


Figure 10: 20-day burst experiment. Time-longitude plot of (a) 0-80 m u (m s^{-1}) and (b) 120-160 m u at the equator; (c) zonal gradient of surface dynamic height (10^{-7} m s^{-2}) with respect to 500 m and (d) same as (c) but for dynamic height at 120 m. The slopes of the lines in (c) denote the phase speeds of the fastest Kelvin (2.4 m s^{-1}) and Rossby (0.8 m s^{-1}) waves, and (d) are consistent with $n=2$ Kelvin and Rossby wave speeds

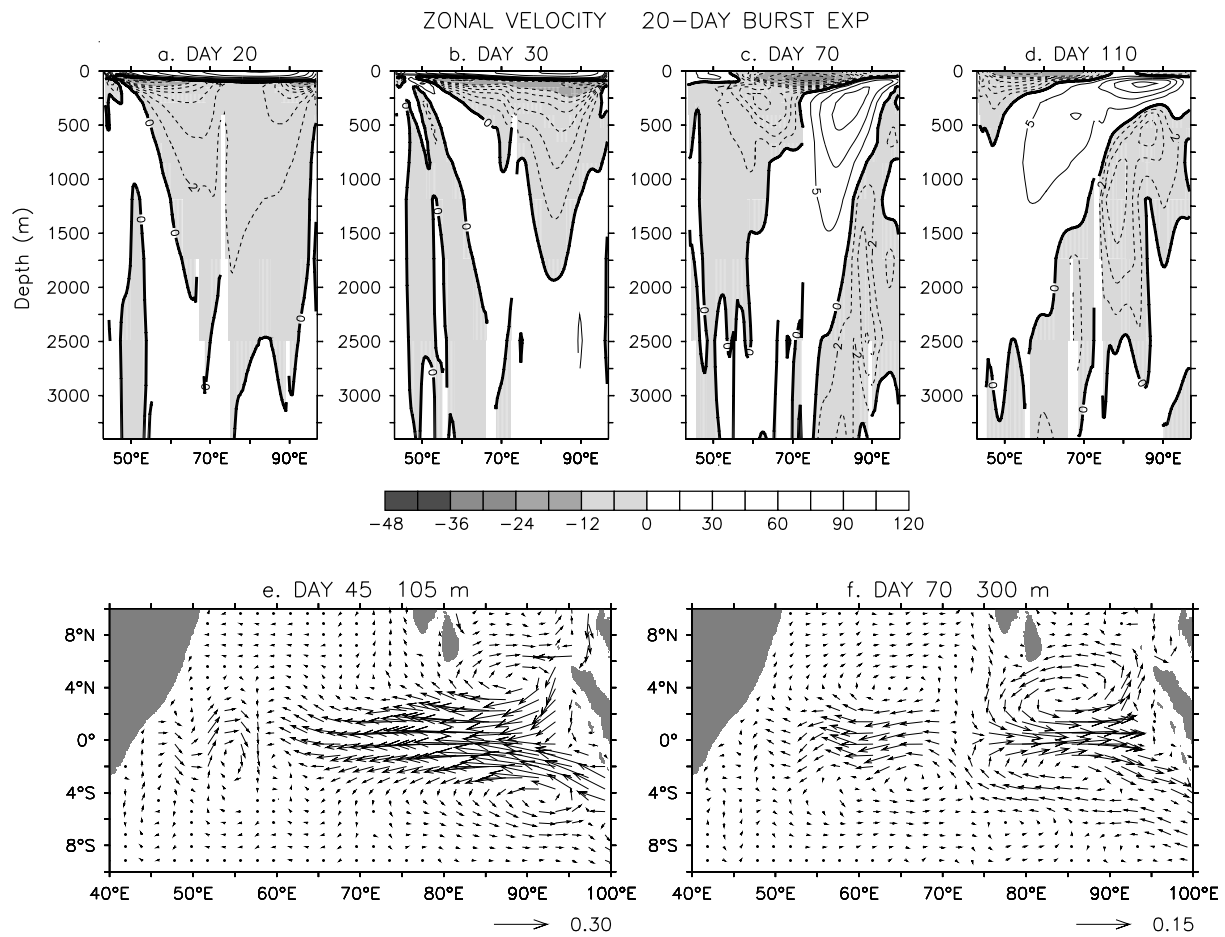


Figure 11: Depth-longitude structure of u (m s^{-1}) at the equator from the 20-day burst experiment, on (a) day 20 (b) day 30 (c) day 70 and (d) day 110. Snapshots of horizontal currents, on (e) day 45 at 105 m and (f) day 70 at 300 m.

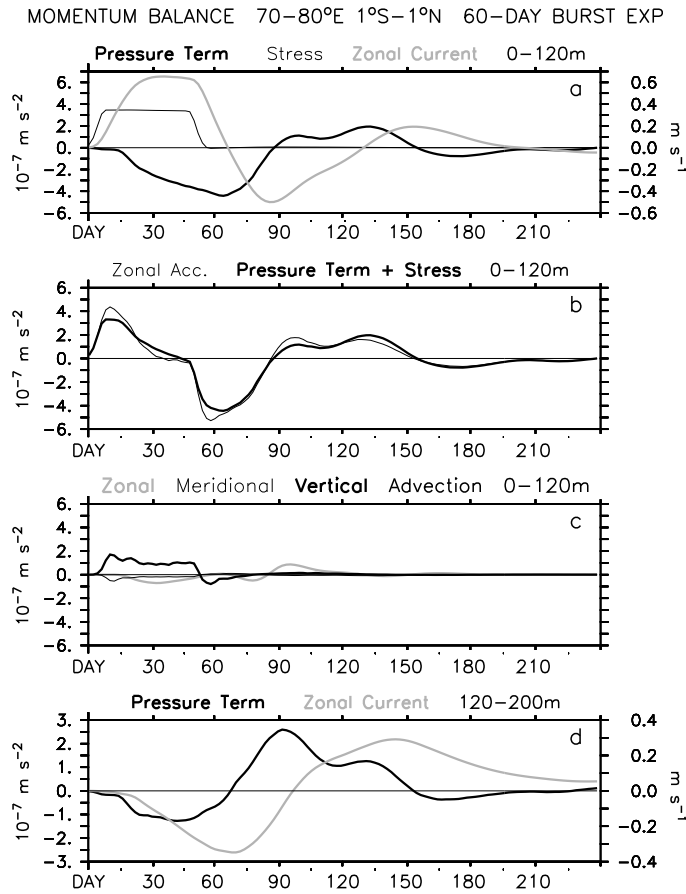


Figure 12: Evolution of terms in the momentum equation in the central Indian Ocean (70–80°E, 1°S–1°N) from the 60-day burst experiment. (a) 0–120m u (grey), pressure term (bold) and stress (thin); (b) 0–120m zonal acceleration (thin) and sum of pressure and stress terms (bold); (c) 0–120m zonal (grey), meridional (thin) and vertical (bold) advection terms; (d) 120–200m pressure term (bold) and u (grey). Units of all terms are 10^{-7} m s^{-2} ; u is in m s^{-1} .

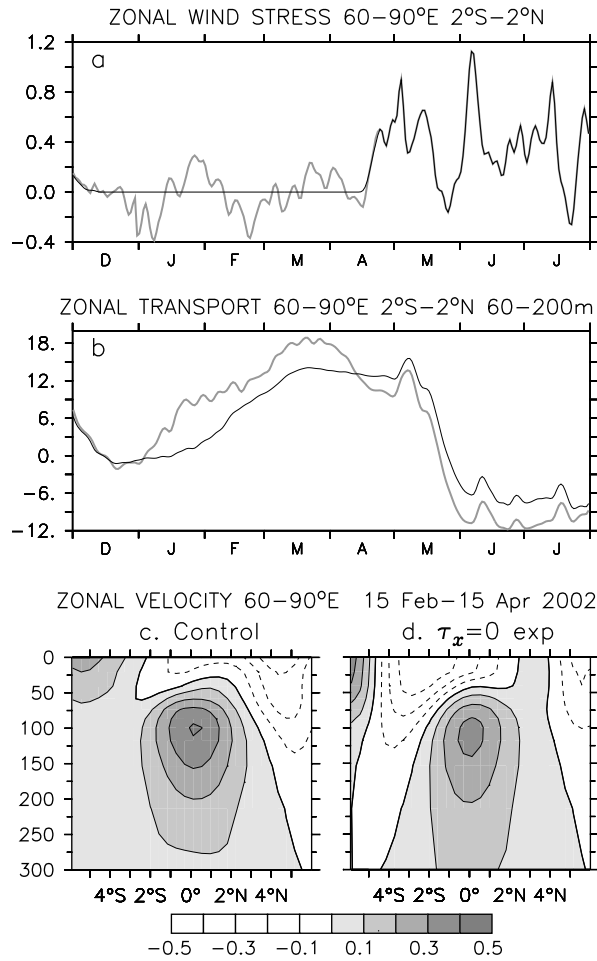


Figure 13: Zonal wind stress and zonal flow in the *control* run (grey) and “Equatorial $\tau_x=0$ experiment” (black). (a) 2°S-2°N, 60-90°E average τ_x (10^{-1} N m^{-2}) December 2001-July 2002 (b) 2°S-2°N, 60-90°E averaged zonal transport (Sv) in the 60-200 m depth range, (c) depth-latitude section of 60-90°E average u (m s^{-1}), (d) as in (c), but for the “equatorial $\tau_x=0$ experiment”.